AALBORG UNIVERSITY

AAU CPH

MSc in Geoinformatics

Monitoring Land Cover Changes using Landsat Data and Maximum Likelihood Classification: A Case Study of Hanoi, Vietnam

Spring 2023 – Masters Thesis

Ana Castellanos Álvarez

June 2, 2023

Abstract

The present study examines the land cover changes in Hanoi, Vietnam, focusing on two distinct time periods: 2000 to 2022 and 2010 to 2022. To conduct this analysis, three satellite images from different periods were acquired: Landsat 7 (ETM+) in 2000, Landsat 5 (TM) in 2010, and Landsat 9 (OLI-2/TIRS-2) in 2022. The methodology employed a Supervised Classification approach utilising the Maximum Likelihood Classifier (MLC) and ArcGIS Pro Software.

The MLC algorithm produced land cover maps with overall accuracy rates of 79, 84, and 84 per cent, respectively. The land cover classes were categorised into four distinct classes: water, built-up land, green areas, and barren land. The findings indicate an expansion of built-up areas by approximately 24 square kilometres from 2000 to 2010, followed by a further increment of approximately 54 square kilometres from 2010 to 2022. In contrast, the green areas exhibited an opposite trend, experiencing a reduction in extent of nearly 56 square kilometres in the first study period and around 10 square kilometres in the second period.

These results suggest that the majority of urban expansion occurred during the period from 2010 to 2022, indicating a notable trend in Hanoi's urban development.

Keywords: Landsat, GIS, Maximum Likelihood Classification, land cover classification, change detection.

Title:

Monitoring Land Cover Changes using Landsat Data and Maximum Likelihood Classification: A Case Study of Hanoi, Vietnam.

Project Period:

January 2023 – June 2023

Student:

Ana Castellanos Álvarez (20212508)

Supervisor:

Dr. Irma Kveladze

Number of Pages:

43

Department:

Department of Development and Planning

Address:

A.C. Meyers Vænge 15, 2450 Copenhagen SW, DK

Acknowledgements

First and foremost, I would like to express my sincere gratitude to my supervisor Dr. Irma Kveladze for her support and guidance throughout the extent of this thesis and for her availability at any time in need.

I would also like to thank Prof. Dr. Jamal Jokar Arsanjani for his assistance regarding remote sensing.

Finally, I would like to thank my family and friends, who have provided moral support and motivation during the challenging times of this thesis.

Table of Contents

List of Figures

List of Tables

List of Equations

List of Abbreviations

ETM+	Enhanced Thematic Mapper Plus
GIS	Geographic Information System
LaSRC	Land Surface Reflectance Code
LEDAPS	Landsat Ecosystem Disturbance Adaptive Processing System
LULC	Land Use/ Land Cover
MLC	Maximum Likelihood Classifier
MSS	Multispectral Scanner
NDVI	Normalized Difference Vegetation Index
NIR	Near Infrared
OLI-2/TIRS-2	Operational Land Imager sensor 2/Thermal Infrared Sensor 2
RS	Remote Sensing
SLC	Scan Line corrector
SR	Surface Reflectance
ST	Surface Temperature
SVM	Support Vector Machine
SWIR	Shortwave Infrared
TM	Thematic Mapper
USGS	United States Geological Survey
WI	Water Index

1. Introduction

At the end of the 20th century, it has been an enormous urbanization acceleration in Asia, increasing over a billion people the population in its cities from 1980 to 2010 (ADB and IDB, 2014), estimated a rise of another billion people by 2030 (ADB and IDB, 2014). Asian urban population increased from 31.5 per cent in 1990 to 42.2 per cent in 2010, the highest percentage increase globally (UN-Habitat, 2012). According to the Asian Development Bank, the level of urbanization in Asia was over 40 per cent in 2018 (United Nations, 2018a), and the projection for 2050 will be up to 60 per cent (ADB and IDB, 2014).

Vietnam did not start significantly increasing its urban population until 1986 when the Doi Moi (which means renovation in Thai) policy was adopted (Phuc, 2013). This reform promoted socioeconomic development and integration with the global economy (Luan et al., 2000). Collectivization was abandoned, returning to self-managed family farms, recognizing households as the basic unit of agricultural production with more rights and security of tenure over their owned land (Kien and Heo, 2008). This policy also stopped price controls and encouraged privatization, removing restrictions on the market and trade-related activities, allowing to develop of foreign investment and fostering trade connections with the rest of the world (Kien and Heo, 2008). After the Do Moi policy promoted industrialization and urbanization, quick changes in the national economic structure occurred (Phuc, 2013).

Weber and Puissant (2003) define urbanization as modifications in a region's territorial and socioeconomic progress, including land cover transformation or land use classification. In terms of physical expansion, housing construction, water surface, vegetation coverage, and infrastructure conditions such as roads and streets are the elements that change when increasing urbanization, being critical factors for monitoring the development of a city (Duan and Shibayama, 2009). During the urban transition, agricultural lands and green spaces typically decrease due to their conversion into residential areas, increasing the housing and road density (Duan and Shibayama, 2009). This conversion in Vietnam was heavily concentrated on two megacities, Hanoi and Ho Chi Minh City (Labbé, 2010), and other medium-sized cities such as Da Nang, Hue, and Dong Nai at a lower scale (Phuc, 2013).

To achieve the urban development intended with this reform, converting agricultural land into built-up areas was necessary since there was little available land (Phuc, 2013). Shifting to an urban society through rural-urban migration, physical expansion of the urban areas, and new cities in rural areas (Labbé, 2010).

The urban population in Vietnam increased from 23.7 per cent in 1999 to 29.6 per cent in 2009 (The Central Census Steering Committee, 2010). Between 1990 and 2018, Vietnam doubled its urban population (United Nations, 2018a), and the UN predicted that by 2050 its population will be up to 60 per cent (United Nations, 2018a).

In Vietnam, between 2002 and 2021, GDP per capita increased 3.6 times and is projected to grow to 6.3 per cent in 2023 (The World Bank, 2023). The poverty rate declined from 14 in 2010 to 3.8 per cent in 2020 (The World Bank, 2023). The agriculture sector has contributed to economic growth and guaranteed food security growing from 2.5 to 3.5 per cent per year over the last three decades (The World Bank, 2023).

Having knowledge about growing patterns can guide planners, policymakers, and others involved in the development process to create equal and environmentally low-impact urban spaces, ensuring more sustainable development of the cities (UN-Habitat, 2012). Monitoring land use/land cover (LULC) changes through the years is a helpful tool to obtain insight into these urban growth trends and the progress in the field of remote sensing (RS) and technologies connected to that has enabled the acquisition of valuable spatiotemporal information regarding that topic (Manandhar et al., 2009).

1.1 Literature Review

Many researchers have focused on LULC changes, which are gaining recognition as a primary cause of environmental changes that impact most regions of the world (Manandhar et al., 2009). A way to study the patterns in urbanization is by mapping LULC changes by combining RS and Geographic Information Systems (GIS). However, the terms land use and land cover are sometimes interchangeable since they do not refer to the same concepts (Lillesand et al., 2015). The term land cover refers to the different types of features present on the surface of the Earth, such as lakes, trees and grass being ordinarily able to be directly mapped from remote sensing images (Lillesand et al., 2015). However, the term land use refers to how humans use land, for example, urban and agriculture (Congalton and Green, 2019). Nevertheless, knowledge of both can be helpful for land planning and land management activities (Lillesand et al., 2015).

In the field of planning and land management, several image classification techniques and algorithms have been adopted (Gao and Mas, 2008). One of them is the pixel-based classification technique that classifies the image based on every single pixel (Dean and Smith, 2003), being able to use supervised, unsupervised and hybrid methods (Enderle et al., 2005). Another method is the object-oriented image classification, which classifies the image by segments, including clusters of pixels with similar spectral characteristics such as segment size, shape, and texture, instead of the individual characteristics of each pixel (Maclean et al., 2013).

Shandas et al. (2017) used RS and GIS to examine the pattern of urban growth in a study case in Doha, Qatar, from 1987 to 2013. They used satellite images acquired from Landsat 4 and 5 TM, Landsat 7 ETM+, and Landsat 8 OLI using a hybrid classification method to detect the land cover of the images. They selected four categories: urban, vegetation, bare soil, and water, for the classification. However, with this method, the percentages of the different accuracies obtained from the confusion matrix were not as high as in other papers that will be mentioned later in this chapter. For example, the producer's accuracy of the urban class and the user's accuracy of the bare soil class was lower than 70 per cent. However, according to them, this is due to the use of similar materials in the construction of rooftops and pavements as those present in the bare soil class, accepting this low level of accuracy owing to the unavailability of other relevant data to enhance the outcomes, as well as the lack of previous studies (Shandas et al., 2017). Additionally, they computed the growth rate based on the land cover classifications to analyze the spatiotemporal expansion of urban areas. They performed a comparative analysis by combining data from various time intervals within the study period using mathematical techniques. In conclusion, they state that physical growth can be visualized by analyzing satellite images using ArcGis 10.2. software. However, additional research is needed to comprehend the urban growth's consequences on social, economic, and environmental factors (Shandas et al., 2017).

Another case study that focuses on investigating the potential of Landsat imagery for assessing the LU/LC changes from 1996 to 2017 is the one carried out by Kumar et al. (2020) in Haridwar Region, India. They applied the Maximum Likelihood Classifier (MLC) method to classify the satellite images into seven classes: orchards, vegetation, agricultural land, rangeland, urban land, water bodies, and watershed. As a result, they obtained overall accuracies of over 80 per cent. Based on the classification obtained from the satellite images, the percentages of changes in the land cover classes and the rate of changes were calculated. They concluded that the outcome of their study was helpful in LU/LC monitoring, decision making and urban planning (Kumar et al., 2020).

In some cases, satellite images are supported by ancillary data for a better understanding of urban growth patterns, as in the case of the paper written by Nong et al. (2015), where they used population data to analyze the relationship between population changes and urban spatial growth. They map land cover changes in Hanoi city and its surroundings using multi-temporal stacks of Landsat Thematic Mapper (TM) and Enhanced Thematic Mapper Plus (ETM+) images from 1993 to 2010 by applying Support Vector Machine (SVM) classifier. Four classes: agriculture, built-up, forest, and water, together with three change classes from agriculture to built-up between three time periods, were created for the study. They analyze the relation of changes in built-up land and the distance from the centre of Hanoi by creating buffer zones of five-kilometre intervals, showing that the significant urban expansion happened between 10 and 25 kilometres from the city centre. In addition, they also show that the most significant increase in population density happened in the peri-urban and rural areas in a 10-kilometre radius around the city centre. The user, producer, overall accuracies, and the kappa coefficient obtained from the confusion matrix were over 90 per cent. However, they found some limitations in using Landsat data, lacking the opportunity for a more detailed mapping, which could give a better understanding of urban pattern analysis (Nong et al., 2015). For example, it was impossible to differentiate between agricultural and green vegetation expansion or between industrial and residential areas (Nong et al., 2015). Furthermore, their study only monitored changes until 2010, so they call for the need for further research to evaluate how the policy objectives outlined in the master plan for Hanoi, which has planned a horizon of 30 years and a projection for 50 years, are impacting urban growth patterns and its potential consequences more accurately (Nong et al., 2015).

Mauro (2020) mapped the urban transformation in Hanoi city and its surroundings using Landsat Imagery from 1989 to 2019. However, MLC was employed in this study in contrast to the previous case study by Nong et al. (2015), where SVM classification was used. Seven classes were established: water, vegetated areas, bare soil, cultivated areas, irregular built-up areas, urban areas, and industrial areas. To analyze the rural-urban conversion, a GIS-based buffer analysis was applied, like the approach used in the study by Nong et al. (2015), which involves the creation of two circles from the city centre with a radio of 10 and 20 kilometres. Classification maps were created for each image, which were later compared. The overall, user and producer accuracies and the kappa coefficient obtained from the confusion matrices were over 80 per cent, except for the user and producer accuracies of the industrial and commercial classes, which were the less common classes. In addition, for a better understanding of urban dynamics, some spatial indexes such as the rate of urban expansion, landscape metrics and the landscape expansion index were calculated. Mauro (2020) found that Hanoi has experienced impressive growth within the examined timeframe, and its surrounding areas are no longer as exclusively rural as they used to be. According to this study, the extension of cultivated areas decreased by 16 per cent between 1989 and 2019. Additionally, rural areas are more fragmented and irregular compared to 1989. On the other hand, urban areas, irregularly built-up areas, and industrial or commercial zones have increased by 20 per cent since 1989 (Mauro, 2020).

Duan and Shibayama (2009) also focus on the urban spatial growth of Hanoi based on RS and GIS. Additional ancillary road and house density data supplemented Landsat images to analyze the urban growth pattern. Moreover, statistical data such as the population of Hanoi were considered, and indices such as the Normalized Difference Vegetation Index (NDVI) and Water Index (WI) were calculated. According to Duan and Shibayama (2009), these index maps provided an effective way for detecting the urban growth of the city, as the reduction in numbers and size of water bodies could be visualized, which is a common phenomenon of urbanization process (Duan and Shibayama, 2009). These maps also allowed the visualization of urbanized areas, their expansion directions, and the decrease or disappearance of greenery and water bodies (Duan & Shibayama, 2009). The supervised MLC method was used to classify land cover in the four Landsat images chosen for the case study. Defining five land cover classes: water, vegetation, built-up, fallow and sand. They quantified the land cover changes by associated change matrices telling how much a class has been changed into another. Nevertheless, the accuracy assessment for the results was not presented in this paper.

According to the literature review findings, supervised classification methods have been extensively employed in land use and land cover mapping. However, the accuracy of these methods varies based on various factors, including the landscape complexity of the study area, the choice of remote sensing data, and the image processing and classification techniques utilized (Lu and Weng, 2007).

1.2 Problem Statement

The rapid urbanization in Hanoi is leading to an increasing loss of agricultural land, causing concern not only for the food security of the inhabitants but also among peri-urban farmers who are worried about their livelihoods (Pham et al., 2015). In addition, housing issues have become increasingly critical due to many factors, including population pressure, rising housing demands, limited land resources, and difficulties in planning and managing urban residential areas (Luan, 2014). Furthermore, the lack of schools, hospitals, water and electricity and the congested traffic is part of the consequences of the rapid increase in the population (Phuong et al., 2021). Moreover, critical environmental problems also emerged from the fast physical growth of the cities, existing a remarkable connection between growth patterns and ecological consequences (Dunlap and Jorgenson, 2012).

For all these reasons, monitoring land cover changes is an important task to perform as it can help understand the dynamics and spatial patterns of urban expansion (Makido and Ferwati, 2017). Moreover, knowing how, when, and where urbanization occurs enables planners and policymakers to evaluate the impact of new policies and make appropriate modifications to foster sustainable growth and reduce potential environmental, social, and economic issues (Nong et al., 2015).

1.3 Research Objective and Research Questions

Based on the problem statement, this thesis aims to explore the suitability of free open-access Landsat satellite data and ArcGIS Pro software to monitor and analyze land cover changes, especially in built-up and vegetated areas in Hanoi, Vietnam. First, land cover classification maps will be created using Landsat imagery from 2000, 2010, and 2022 and a supervised classification method. Subsequently, land cover change maps will be generated based on these classification maps, enabling visual observation of the changes between land cover classes within two distinct time periods: 2000 to 2010 and 2010 to 2022. Moreover, the areas of the different land cover classes and the land cover changes will be quantified to analyze these changes.

To accomplish the stated objectives, the following research questions should be addressed:

1. Is Landsat data suitable to classify land cover in Hanoi using Maximum Likelihood Classifier?
    a. How does MLC perform in monitoring land cover using Landsat spectral bands?
    b. How does the Normalized Difference Vegetation Index perform in monitoring land cover by establishing the corresponding thresholds for the different classes?
2. Are the land cover classifications suitable to detect land cover changes in Hanoi?

2. Study area, Data Collection and Software

2.1 Hanoi Overview and the Study Area

Hanoi, the capital of Vietnam, is located in the centre of the Red River Delta region at a longitude of 106 degrees East and latitude of 21 degrees North, being the second largest city in the country after Ho Chi Minh City (Word Population Review, 2023). The current population is 5.25 million, having experienced a population growth of 3.67 per cent from the previous year (Word Population Review, 2023). The administrative boundaries of Hanoi province were modified several times through the twentieth century (Labbé, 2021). In 2008, Hanoi experienced a considerable expansion by including the neighbouring area of Ha Tay and some districts from the neighbouring province of Vinh Phuc and Hoa Binh (Labbé, 2021), triggering not only an incrementation in Hanoi's extension from 900 to 3328.9 square kilometres (Word Population Review, 2023) but also doubling its population (Labbé, 2021).

The population density in Hanoi was 2.031 persons per square kilometre in 2011, rising to 2.480 in 2021 (GSO, n.d.) These statistics present challenges in terms of providing accessible recreational spaces and green areas within the city, as well as highlighting the unequal distribution of such amenities (Labbé, 2010). The largest parks are primarily located in the periphery, making them hardly accessible from the inner city due to the poor public transport connections (Labbé, 2021). By 2010, Hanoi had less than 1.5 square meters of park space per person (Boudreau and Geertman, 2015). Moreover, the area dedicated to green spaces per habitant in 2011 was 11.2 square meters per capita, which is relatively low compared to the Asian average of 39 square meters (EIU, 2011). In 2021, the authorities gave more importance to the role of public spaces and green areas by establishing new planning policies which oblige developers to include 3 to 4 square meters per capita of parks and green areas to be able to obtain permission to build (Labbé, 2021).

The expansion of urban development has had a notable impact on the transportation infrastructure (Labbé, 2021). While the number of cars and motorcycles in the capital has experienced a substantial increase, the public transport system has failed to keep pace with this growth (Labbé, 2021). This is partly due to the Doi Moi reform, which reduced the budget allocated to state-owned companies responsible for public transport development (JICA, 2007). However, the government later shifted its focus towards prioritizing public transportation by approving the "Hanoi Master Plan 2030 and Vision to 2050" in 2011, where eight metro lines, with a total length of about 318 kilometres (Liou et al., 2021), three monorail lines and nine express bus routes were planned to build (Labbé, 2021). Unfortunately, it did not go as expected since only two of the metro lines started in 2021, being several years behind schedule, and only one line of the express bus route was operational in 2021 (Labbé, 2021).

The rapid urbanization and consequent loss of agricultural land in Hanoi and its peripheries make it difficult for the government to deal with the rural-urban conversion (Luan, 2014). To address this issue and reallocate the population from the overpopulated city centre, the government established an urban development model called 'New Urban Areas' (NUA) in 1990 (Luan, 2014). However, these

NUA lacked social infrastructure and connection to the city centre, converting these areas into 'sleeping' towns with a low rate of habitats in 2014 (Luan, 2014). Moreover, the stipulated requirement of allocating 30 to 50 per cent for affordable housing was not achieved (Nong et al., 2015).

The study area includes Hanoi and its surrounding districts within a radius of around 20 kilometres. This extension was chosen based on previous studies, such as the one from Nong et al. (2015), where they showed that the most remarkable urban expansion happened around this extension. This area includes 15 districts: Ba Dinh, Cau Giay, Dong Anh, Dong Da, Gia Lam, Ha Dong, Hai Ba Trung, Hoai Duc, Hoan Kiem, Hoang Mai, Long Bien, Tay Ho, Thanh Tri, Thanh Xuan, Tu Liem. The study area covers an extension of 747.85 square kilometres (Figure 1).

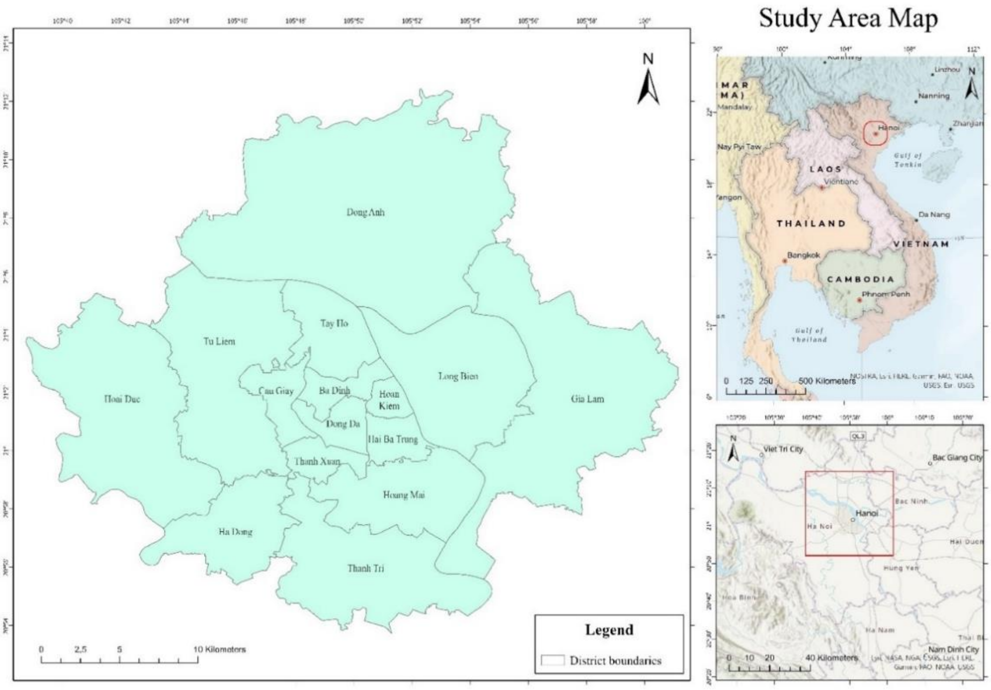

Figure 1. Study Area and its location.

2.2 Data Collection

2.2.1 Satellite Imagery

The urban growth analysis of the study area has been carried out by selecting three images acquired from Landsat 7 Enhanced Thematic Mapper Plus (ETM+), Landsat 5 Thematic Mapper (TM), and Landsat-9 Operational Land Imager sensor/Thermal Infrared Sensor (OLI-2/TIRS-2) on 04 November 2000, 08 November 2010 and on 19 December 2022, respectively. All Landsat data were obtained from the United States Geological Survey (USGS) through the Earth Explorer platform (https://earthexplorer.usgs.gov/), which became freely available in 2008 (Zhu et al., 2019). Acquiring images at around the same time of the year was essential because seasonal variations can alter the appearance of land use features, such as in crop fields leading to potential inaccuracies in the results (Paul, 2008). Therefore, the images are from the autumn crop season because it is usually the only period with available data without cloud coverage (Mauro, 2020). All the data were acquired from Landsat Collection 2 processing Level-2 (L2) with a cloud cover level of less than 2 per cent (Table 1). In processing Level-2, there are Surface Reflectance (SR) and Surface Temperature (ST) scene-based products, which are specified in each image (USGS, 2020). Landsat 4-7 Collection 2 SR science products are created from a software named Landsat Ecosystem Disturbance Adaptive Processing System (LEDAPS) version 3.4.0, which applies the atmospheric correction to Landsat 4-5 TM and Landsat 7 ETM+ Level 1 (L1) data (USGS, 2020). In the case of Landsat 8-9 OLI/TIRS USGS, a different software called Land Surface Reflectance Code (LaSRC) is used for atmospheric correction (Zanter, 2021). The products with SR are already corrected and ready to be used (USGS, 2020).

Table 1. The satellite image database.

Satellite	Sensor	Processing Level	Date of Acquisition	Spatial resolution	Cloud coverage (%)	WRS Path (P)/Row (R)	UTM Zone/Datum
Landsat 7	Enhanced Thematic Mapper (ETM+)	2	04/11/2000	30m	0	127/045	48N/WGS84
Landsat 5	Thematic Mapper (TM)	2	08/11/2010	30m	1	127/045	48N/WGS84
Landsat 9	Operational Land Imager sensor/Thermal Infrared Sensor (OLI-2/TIRS-2)	2	19/12/2022	30m	0	127/045	48N/WGS84

The image from 2000 was acquired by Landsat 7, launched in April 1999, carrying the Enhanced Thematic Mapper Plus sensor (USGS, n.d.-c). Landsat 7 includes eight spectral bands with different spatial resolutions varying between 15, 30 and 60 meters (Table 2) (USGS, n.d.-c).

Table 2. Spectral features of Landsat-7 bands (USGS, n.d.-c).

Landsat 7	Wavelength (micrometres)	Resolution (meters)
Band 1- Blue	0.45 - 0.52	30
Band 2 - Green	0.52 - 0.60	30

Band 3 - Red	0.63 - 0.69	30
Band 4 - Near Infrared (NIR)	0.77 - 0.90	30
Band 5 - Shortwave Infrared (SWIR) 1	1.55 - 1.75	30
Band 6 - Thermal	10.40 - 12.50	60 (30)
Band 7 - Shortwave Infrared (SWIR) 2	2.09 - 2.35	30
Band 8 - Panchromatic	0.52 - 0.90	15

However, due to a permanent failure in the Scan Line corrector (SLC) of the Landsat 7 (ETM+) in June 2003 (USGS, n.d.-c), the images acquired from this date had data gaps of around 22 per cent of the normal scene area (Storey and Barsi, 2005) (Figure 2). To be able to use the images acquired from Landsat 7 after 2003, the option Fix Landsat 7 Scanline Errors from the Landsat toolbox in ArcGIS (freely downloaded from LandsatToolbox for ArcGIS 10.1 - Overview) can be used to fix the data gap, applying the correction for every single band (Subha, 2020).

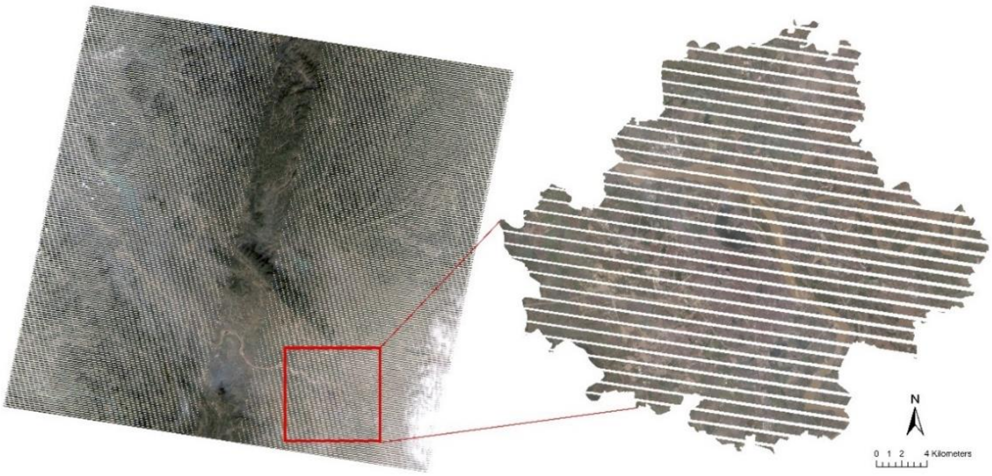

Figure 2. Landsat 7 ETM+ image acquired after the SLC failure. The image on the left is the composite band (1 - 8 except band 6) from the entire data set downloaded from https://earthexplorer.usgs.gov/, and the image on the right is the study area.

The image from 2010 was acquired by Landsat-5, which was launched on March 1984 and was operated until June 2013, carrying the Multispectral Scanner (MSS) and the TM sensors (USGS, n.d.-a). Unfortunately, the MSS sensor with four spectral bands stopped taking images from 1999 until 2011 (USGS, n.d.-a). Hence, for the image captured in 2010, only the TM sensor with seven spectral bands is available. (Table 3) (USGS, n.d.-a).

Table 3. Spectral features of Landsat 5 bands (USGS, n.d.-a).

Landsat 5	Wavelength (micrometres)	Resolution (meters)
Band 1- Blue	0.45 - 0.52	30
Band 2 - Green	0.52 - 0.60	30
Band 3 - Red	0.63 - 0.69	30
Band 4 - Near Infrared (NIR)	0.77 - 0.90	30
Band 5 - Shortwave Infrared (SWIR) 1	1.55 - 1.75	30
Band 6 - Thermal	10.40 - 12.50	120
Band 7 - Shortwave Infrared (SWIR) 2	2.09 - 2.35	30

The image from 2022 was acquired by Landsat-9, which was launched on September 2021 and carried two instruments which are the Operational Land Imager 2 (OLI-2) and the Thermal Infrared Sensor 2 (TIRS-2) (USGS, n.d.-b). The satellite data set includes eleven bands (Table 4).

Table 4. Spectral features of Landsat 9 bands (USGS, n.d.-c).

Landsat 9	Wavelength (micrometres)	Resolution (meters)
Band 1- Coastal aerosol	0.43 - 0.45	30
Band 2 - Blue	0.45 - 0.51	30
Band 3 - Green	0.53 - 0.59	30
Band 4 - Red	0.64 - 0.67	30
Band 5 - Near Infrared (NIR)	0.85 - 0.88	30
Band 6 - Shortwave Infrared (SWIR) 1	1.57 - 1.65	30
Band 7 - Shortwave Infrared (SWIR) 2	2.11 - 2.29	30
Band 8 - Panchromatic	0.50 - 0.68	15
Band 9 - Cirrus	1.36 - 1.38	30
Band 10 - Thermal Infrared (TIRS)1	10.6 - 11.19	100
Band 11 - Thermal Infrared (TIRS) 2	11.50 - 12.51	100

Apart from Landsat imagery, data from the administrative areas were necessary to delineate the study area. This data was freely available from the Database of Global Administrative Areas (http://www.gadm.org/country), a database created in 2009 that provides vector data from all countries at various administrative levels.

2.2.2 Ancillary Data

Several studies, such as the ones performed by Akar and Güngör (2015) or Manandhar et al. (2009), acknowledged that the incorporation of some ancillary data, such as the normalized difference vegetation index (NDVI), can improve the LULC classification accuracy. There are other indices for stressing vegetation areas on remote sensing images (Bhandari et al., 2012), such as Enhanced Vegetation Index (EVI), Perpendicular Vegetation Index (PVI), or Ration Vegetation Index (RVI) (Kshetri, 2018). However, the NDVI is the most commonly used to determine the presence of healthy green vegetation (Manandhar et al., 2009).

This index is based on how plants reflect specific electromagnetic spectrum ranges (Kshetri, 2018). For example, healthy vegetation is green to the human eye because its chlorophyll pigment reflects green spectrum and absorbs the red one (Kshetri, 2018). In contrast, an unhealthy plant reflects the red spectrum and absorbs the green one (Kshetri, 2018). This numerical indicator for vegetation greenness is delivered as a single-band product based on the difference between the red and the near-infrared bands (Kshetri, 2018) calculated by the following formula:

$$NDVI = (NIR - Red) / (NIR + Red) \qquad \text{Equation 1}$$

NDVI values vary from -1 to +1, wherein generally negative values represent water bodies, very low values (up to 0.1) indicate bare soil areas, moderate values represent grassland (0.2 to 0.3), and high values represent dense vegetation or tropical rainforest (Bhandari et al., 2012).

2.3 Software

2.3.1 ArcGIS Pro version 3.0.0.

ArcGIS Pro is a software provided by Esri (https://www.esri.com/en-us/arcgis/products/arcgis-pro/overview), which has been used to achieve the study's objectives.

2.3.2 Google Earth Pro

Google Earth Pro is a software provided by Google that is accessible through the website https://earth.google.com or available for free download from Earth Versions – Google Earth. This software allows access to very high-resolution satellite data and enables to import GIS information. The very high-resolution images displayed in Google Earth Pro have been used as reference data for obtaining the training samples and performing the accuracy assessment. In this case study, the downloaded version was used, as it provides the necessary functionality for accessing historical imagery, which is not available in the online version.

3 Methodology

3.1 Data Pre-processing

An advantage of remote sensing data is the capability to carry out image processing that can enhance or modify the image (Gong and Liu, 2023). Usually, the raw data is not appropriate for direct processing (Gong and Liu, 2023). Therefore, preparation was needed before processing the images, such as band combination and clipping the images to the needed extension. However, other pre-processing actions were not needed. For example, since the images collected from Earth Explorer were from Collection 2 Level-2, they were already atmospherically corrected surface reflectance images (SR). In addition, the cloud pre-processing was also unnecessary as the images were cloud-free. Furthermore, the multiple bands used in the composite band have 30 meters resolution, so resampling was unnecessary.

3.1.1 Bands Combination

The Landsat raster data available from Earth Explorer are single-bands; therefore, the appropriate band combinations should be determined and stacked into a multi-band image (Gong and Liu, 2023). This operation was performed by a data management tool, Composite Bands, from ArcGIS Pro. For the Landsat 5 and Landsat 7 images, the SR visible bands 1-5 and band 7 were used to create the Composite Band raster. Band 6 (ST) is for thermal purposes, and band 8 (only existing in Landsat 7) is a panchromatic band. Both have been considered irrelevant to the study and, therefore, not included. The images are shown as a true colour composite using the red, green and blue bands (bands 3,2,1) (Table 5).

For the Landsat 9 image, the SR visible bands 1-7 were used to create the Composite Band raster. The thermal, panchromatic and cirrus bands were not used as they were considered irrelevant to the study. The image is shown as a true colour composite using the red, green and blue bands (bands 4,3,2).

Table 5. Bands and RGB used in the different images.

Data	Composite	RGB
Landsat 7 ETM C2 L2	1,2,3,4,5,7	3,2,1
Landsat 5 TM C2 L2	1,2,3,4,5,7	3,2,1
Landsat 9 OLI/TIRS C2 L2	1,2,3,4,5,6,7	4,3,2

3.1.2 Image Extraction

The satellite image data acquired from Earth Explorer include a vast, unnecessary area for the research. To reduce the time-consuming and storage space, a new raster with a smaller extension matching the study area was created, excluding the information that falls beyond its limits. To perform that, a spatial analyst tool, Extract by Mask, was performed in ArcGIS Pro software, using the polygon of the study area as a mask data (Figure 6).

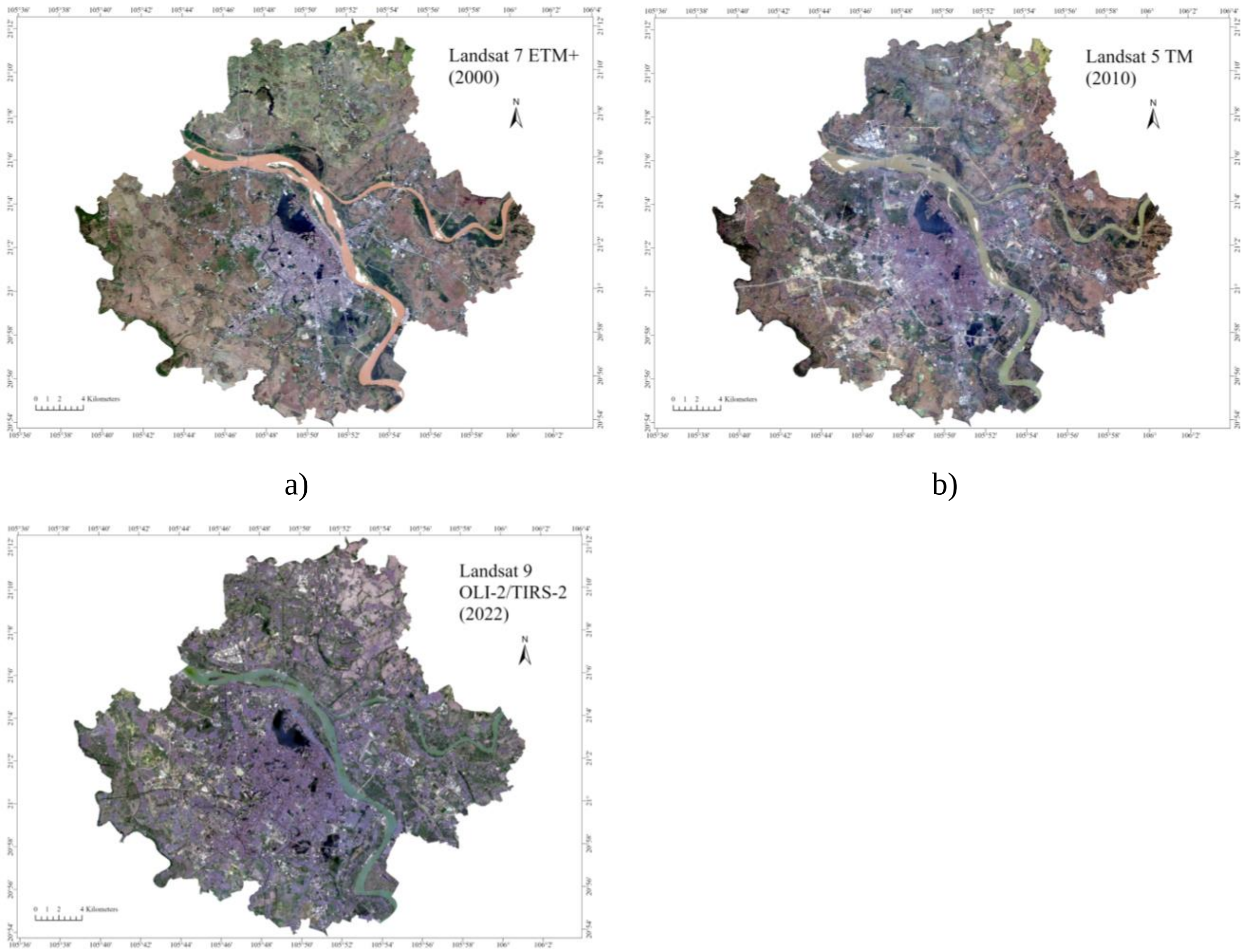

a) b)

c)

Figure 3. Clipped multi-band images of the study area: a) Landsat 7 ETM+ image from 2000; b) Landsat 5TM image from 2010; c) Landsat 9 OLI-2/TIRS-2 from 2022.

3.2 Maximum Likelihood Classification

As a supervised classification method, the Maximum Likelihood Classification algorithm trained the model to establish representative parameters for each land cover class using manually digitized training areas based on very high-resolution data (Lillesand et al., 2015). There is a multitude of very high-resolution data available such as WordView-1 (0.5m), GeoEye-1 (0.5m), QuickBird (1m) and IKONOS (1m), among others (SIC, 2022). However, for this study, Google Earth data were used as reference data due to its availability at a very high resolution without any cost. Once the training samples are created, the algorithm will assign each pixel to the land cover class that looks most like it. The pixel, which is unlike any training area, will be categorized into an "unknown" class (Lillesand et al., 2015).

The main objective of image classification is to automatically classify all pixels into surface feature categories. This is typically achieved by gathering pixels with similar spectral reflectance combinations, known as spectral patterns, that supposedly represent the different land cover classes without considering the surrounding pixels (Lillesand et al., 2015).

To define the land cover classes, the classification system used by the United States Geological Survey (USGS) based on the Anderson system was used as a model (Anderson et al., 1983). This standard classification includes four different levels of information, depending on the degree of detail that can be obtained due to the sensor system and image resolution (Lillesand et al., 2015). Level I is for low to moderate-resolution satellite data such as Landsat Multispectral Scanner system (MSS) data, and level II is for small-scale and moderate-resolution satellite data such as Landsat TM data (Anderson et al., 1983). Both levels are generally for mapping information across the country, multiple or entire states (Lillesand et al., 2015) (Table 7).

Table 6. USGS Land Use/Land Cover Classification System with Levels I and II of information for use with Remote Sensor Data (Anderson et al., 1983).

Level 1	**Level II**
1 Urban or built-up land	11 Residential 12 Commercial and service 13 Industrial 14 Transportation, communications, and utilities 15 Industrial and commercial complexes 16 Mixed urban or built-up land 17 Other urban or built-up land
2 Agricultural land	21 Cropland and pasture 22 Orchards, groves, vineyards, nurseries, and ornamental horticultural areas 23 Confined feeding operations 24 Other agricultural land
3 Rangeland	31 Herbaceous rangeland 32 Shrub and brush rangeland 33 Mixed rangeland
4 Forest land	41 Deciduous forest land 42 Evergreen forest land 43 Mixed forest land
5 Water	51 Streams and canals 52 Lakes 53 Reservoirs 54 Bays and estuaries

6 Wetland	61 Forested wetland 62 Nonforested wetland
7 Barren land	71 Dry salt flats 72 Beaches 73 Sandy areas other than beaches 74 Bare exposed rock 75 Strip mines, quarries, and gravel pits 76 Transitional areas 77 Mixed barren land
8 Tundra	81 Shrub and brush tundra 82 Herbaceous tundra 83 Bare ground tundra 84 Wet tundra 85 Mixed tundra
9 Perennial snow or ice	91 Perennial snowfields 92 Glaciers

Level III is suitable for a resolution of 1 to 5 meters, and level IV is even higher (Lillesand et al., 2015). However, for both of these levels, ancillary data must be added to the imagery data to be able to classify at that precise level (Lillesand et al., 2015). An example of the detail of the classes in Level III is shown in the table below (Table 8).

Table 7. Level III of information on USGS Land Use/Land Cover Classification System for Use with Remote Sensor Data (Anderson et al., 1983).

Class name	Class Description
11 Residential	111 Single-family 112 Multifamily 113 group quarters 114 Residential hotels 115 Mobile home parks 116 Transient lodgings 117 Others

In this case study, level I is applied for the classification, as the sub-classes described in level II are too specific and irrelevant to the case (Table 9).

Table 8. Land cover classes delineated for the classification.

Class name	Class Description
Water bodies	Streams and canals, lakes, reservoirs and bays and estuaries
Built-up land	Residential, commercial, industrial, roads and transportation, communications and utilities
Green areas	Green areas, cropland and pasture
Barren land	Beaches, sandy areas, open fields without vegetation, exposed rocks, gravel pits, transitional areas

3.2.1 Training Samples

The first step in performing the supervised classification is creating the training samples, which consist of collecting the representative ground truth of the different land cover areas to create a numerical definition of the spectral attributes of each land cover class (Lillesand et al., 2015). To create the training samples, reference data and/or knowledge of the geographic area is needed (Lillesand et al., 2015). Reference data from Google Earth Pro has been used in this case study for being very high-resolution data and freely accessible.

The quality of this process will define the accuracy of the classification, being of great importance the creation of representatives and complete training samples for all the required land cover classes (Lillesand et al., 2015). Through the training process, it will gather a set of statistics that define all spectral classes that each land cover class has (Lillesand et al., 2015).

Training samples were created through Training Samples Manager from the Image Classification tool in ArcGIS Pro, drawing polygons manually over the areas of each land cover class using Google Earth Pro as reference data. To visualize reference data from the years 2000, 2010 and 2022 on Google Earth Pro, the time slider icon was used. In some cases, it was impossible to find an image for the specific period of study. For example, in the image below, the closest date available as reference data was February 2010, although this study required reference data from November 2010 (Figure 4).

Figure 4. Time slider to find historically imaginary.

These polygons have been drawn, preventing pixels near the borders between land cover types. In addition, they were delineated throughout the whole study area to increase the chance of being representative (Lillesand et al., 2015). The number of reference samples that have been created resulted in a total of between 275 and 300 for each image, with different samples for each land cover class (Figure 5).

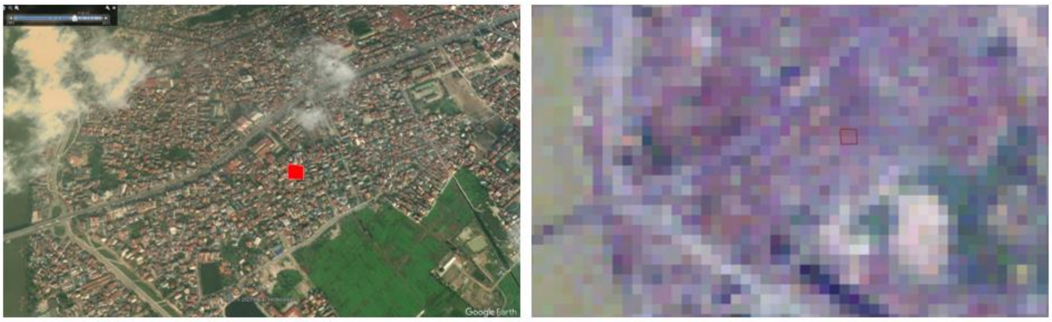

a) b)

Figure 5. Example of a built-up training sample: a) Reference data from Google Earth Pro, 2010; b) Landsat image 2010.

As a part of the training process, an evaluation of the quality within the samples of each class is performed (Lillesand et al., 2015). One approach for addressing this is visualizing the histograms for each training class in the different bands, which show the distribution of pixels of the individual classes. The desired outcome of the histogram analysis is to observe a Gaussian distribution or close to it, indicating a normal distribution in all the bands (Lillesand et al., 2015). The histograms are performed in ArcGIS Pro by creating a clipped raster for each land cover class. So for every composite image, four different clipped rasters were created. In doing so, only the training sample of that specific class is analyzed, performing a histogram for each band, as shown in the example below (Figure 6).

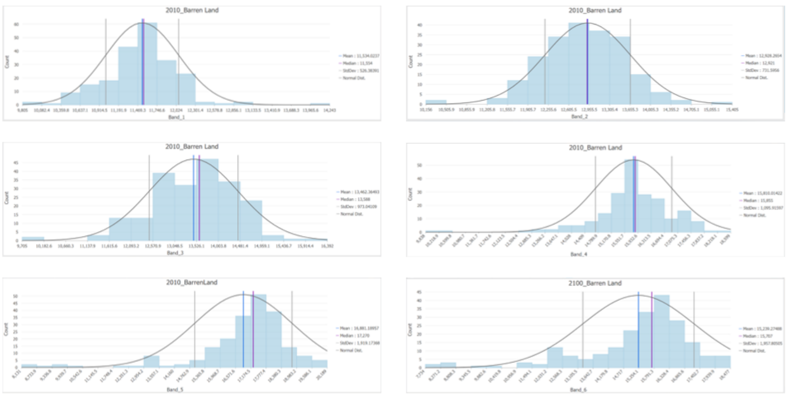

Figure 6. Histograms for the training samples barren land for Landsat image 2010, showing the histograms of every band.

However, the histograms do not show the comparison between the different classes. To do that, a spectral separability plot can be performed (Lillesand et al., 2015). In this plot, the average pixel value from the training polygons of each class is shown, as well as the error bar that represents the standard deviation. The figure tells whether or not two different classes will be separable and which bands will be the most helpful. For example, the figure below, representing the spectral separability plot for the training samples from the Landsat image 2010, shows that all the classes look very similar in band 1, which means that this band is not going to be that helpful in separating the classes as, for example, could be band 4, as it is more spread in the values (Figure 7).

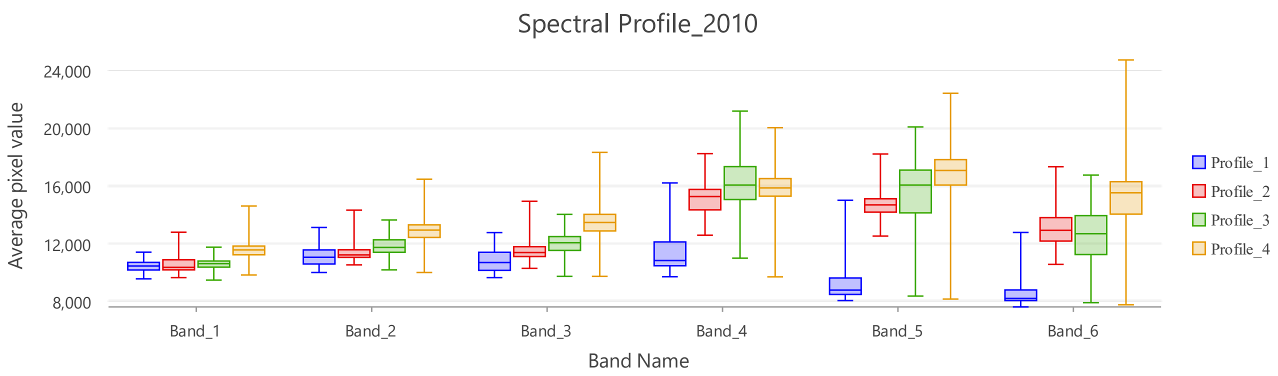

Figure 7. Spectral separability plot for training samples of Landsat image 2010. Profile_1 represents water, profile_2 built-up land, profile_3 green areas, and profile_4 barren land.

Another approach for evaluating the quality of the training samples within each class is to examine the error matrix, which reveals the percentage of the training pixels that are correctly classified, providing insight into the accuracy of the classification process (Lillesand et al., 2015). The description of the error matrix will be elaborated upon in Chapter 3.5. This evaluation is conducted once the classification process is completed (Lillesand et al., 2015).

3.3 Post-processing

The outputs from the pixel-based classification need some post-classification operation before a further process. The classification outputs show some isolated misclassified pixels that differ from their neighbouring pixels, known as salt-and-pepper noise (Lillesand et al., 2015). This noise is due to similarities in the spectral responses of specific land cover classes (Lillesand et al., 2015). These misclassified pixels can be removed using the majority filter tool in ArcGIS Pro software to get a smoother image showing an outcome of the predominant classification, being the one supposedly correct. Using this tool, each pixel is replaced by the value of the majority of its neighbours, being able to choose between four or eight neighbours (Esri, n.d.-b). For this case study, eight neighbours and the majority option for the replacement threshold were chosen to perform the image post-processing.

3.4 NDVI

An NDVI was calculated for each multispectral image using ArcGIS Pro Software's raster functions. The red and near-infrared bands were used to obtain the single band dataset, following equation 1 described in Chapter 2.2.2. To calculate the NDVI for the images from 2000 and 2010, acquired from Landsat 7 and 5, respectively, the fourth band (near-infrared) and the third band (red) were used. In the case of the 2022 image obtained from Landsat 9, the fifth band (near-infrared) and the fourth band (red) were used.

Defining the thresholds for each class was necessary to generate a cover classification map based on NDVI values. Therefore, the "classify" symbology was employed, categorizing the classes into water, non-vegetated and vegetated. To establish these thresholds, reference data were used to determine the values associated with each class. The corresponding reference data was obtained through the icon time slider in Google Earth Pro and subsequently imported into ArcGIS Pro. Georeferencing the imported image was performed by adding control points. To ensure accurate georeferencing, strategic points located along the borders of the study area were used as control points due to this delineation was also present in the image imported from Google Earth Pro.

3.5 Accuracy Assessment

The history of accuracy assessment for maps generated from spatial data is relatively short, beginning in 1976 when the first standard for the minimum level of accuracy assessment of LULC classification from remote sensor data was proposed by Anderson et al. (1983), estimated at least 85 per cent to be considered adequate. However, this threshold was established without any study demonstrating that this value was the most acceptable (Congalton and Green, 2019). After that, some studies proposed fundamental approaches for testing accuracy assessment, as by Hord and Brooner (1976) and Ginevan (1979). Finally, at the beginning of the 1980s, researchers such as Rosenfield et al. (1982), Congalton et al. (1983) and Aronoff (1985), among others, proposed more elaborated techniques, being from the end of the 1980s until today when the amount of research about it has highly increased, certifying that the perform of the accuracy assessment is necessary for all remote sensing mapping projects (Congalton and Green, 2019).

According to Congalton (2001), presenting just the creation map as a final result is insufficient for a complete and valid classification map using spatial data. Instead, it is necessary to perform an accuracy assessment to know how well the classification has been performed and to increase the quality of the map information by interpreting the assessment (Congalton, 2001). In addition, it allows for comparing different methods quantitatively (Congalton, 2001).

Congalton (1988) recommended a minimum of 50 samples per class for maps containing up to twelve classes and an area of fewer than one million acres; otherwise, more samples will be required. In general, the number of samples for each class should be adapted depending on how important the specific class is for the project, as well as being aware that the more versatile classes require more samples than the classes that show fewer variables as, for example, water (Congalton and Green, 2019). For the sampling strategy, there are three options: stratified random, equalized random and random (Esri, n.d.-a). With the random sampling strategy, the points will be randomly distributed through the image with no criteria, while with the stratified random sampling strategy, each class is assigned a number of points proportionately to its corresponding relative area (Esri, n.d.-a). In contrast, in the equalized stratified random sampling strategy, all the classes will have an equal number of points (Esri, n.d.-a). The accuracy assessment points in the case study were established through the Image Analyst Tool, 'Create Accuracy Assessment Points' in ArcGIS Pro, choosing 200 random points and the stratified random sampling strategy.

After creating the accuracy assessment points, the correct classification for each point was manually assigned by checking the reference data. To accomplish this, the shapefile containing the accuracy assessment points was exported to Google Earth Pro after being converted to a KML file (Figure 8).

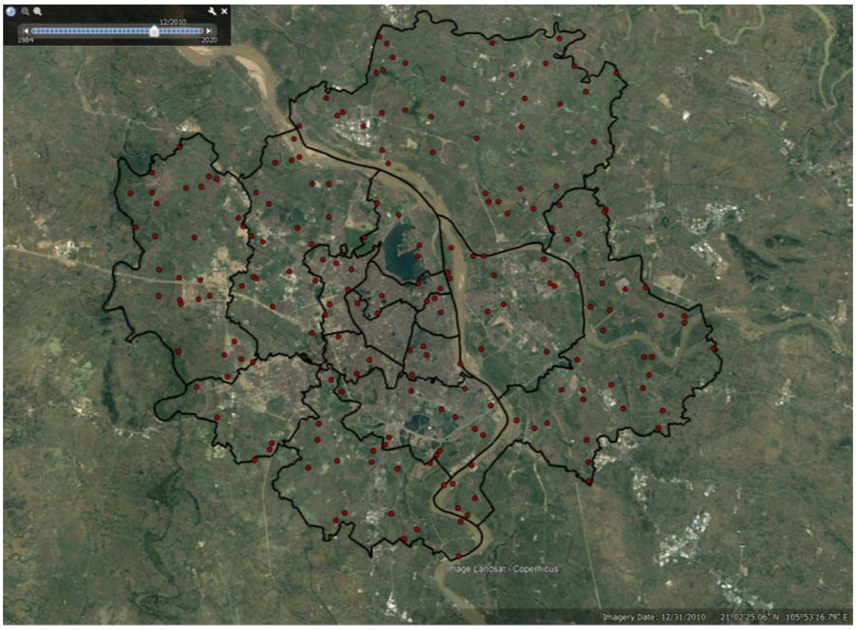

Figure 8. Accuracy assessment points. The points were generated in ArcGIS Pro and subsequently exported to Google Earth Pro for conducting the assessment with the reference data.

The most common method used in the remote sensing community to assess accuracy is to compute the confusion or error matrix (Congalton and Green, 2019), which was calculated using the Image Analyst Tool, Compute Confusion Matrix in ArcGIS Pro.

The confusion matrix is a square array where the number of rows and columns is the same as the number of classes that are being assessed, indicating the number of sample units assigned to a particular class (Congalton, 2001). The relationship between known reference data or ground truth data, represented in the columns, and the corresponding result of the classification, represented in the rows, is compared class by class (Congalton and Green, 2019). Through the confusion matrix is possible to know the commission and the omission errors. The commission error is the one that happens when an area is included in a class to which it does not belong, while an omission error is the one that happens when an area is excluded from the class to which it truly belongs (Congalton and Green, 2019). In addition, several accuracies can be calculated from the confusion matrix: the overall, the user and the producer's accuracy. The overall accuracy is calculated by dividing the total number of correctly classified pixels, which are the ones located in the main diagonal, by the total number of reference pixels in the confusion matrix (Congalton and Green, 2019). According to Congalton and Green (2019), evaluating the different classes that intervene in the classification is necessary, as it is not enough only show the overall accuracy to represent the classification's accuracy. To evaluate the different classes, the producer and the user's accuracy must be shown (Congalton and Green, 2019). The producer's accuracy gives the producer an idea of the correct classification for each class by indicating the probability of a reference sample is correctly classified and being a measure of omission error (Congalton, 2001). This accuracy is calculated by dividing the number of correctly classified samples in each class, the value located on the main diagonal, by the total number of samples of that specific class, the value located in the column total (Congalton and Green, 2019). The user's accuracy indicates the measure of commission error by expressing the probability that a sample classified on the map represents that class on the ground (Story and Congalton, 1986). This is calculated by dividing the number of correctly classified samples in each class, the value located on the main diagonal, and the total number of samples used for the specific class, the value in the row total.

Another value estimated from the confusion matrix is the K statistics or Kappa coefficient, widely used in classification accuracy assessment (Foody, 2020). This coefficient is an indicator of the extent to which the percentage correct values of an error matrix can be attributed to "true" agreement versus "chance" agreement, and its value ranges between 0 and 1 (Lillesand et al., 2015). However, despite its widespread use, there are many concerns about its application in accuracy assessment to the extent of calling, unsuccessfully, to abandon its use (Foody, 2020). In fact, Olofsson et al. (2014) consider using the kappa coefficient as poor practice in accuracy assessment, which consists of the suggestions of Strahler et al. (2006), who discouraged its use due to its limited significance in accuracy assessment. Furthermore, Foody (2020) conducted a study demonstrating the unsuitability of the kappa coefficient to describe the accuracy and its comparison. Foody (2000) provided an example where a classification with an overall accuracy of 95% could have a kappa coefficient ranging from 0.026 to 0.900, highlighting the lack of utility in determining assessment accuracy.

3.6 Land Cover Change Detection

Change detection was performed to identify, visualize and analyze land cover changes in the study area for two time periods. One analysis focused on land cover changes between 2000 and 2010, while the other examined changes between 2010 and 2022, with a calculation of the corresponding areas for these changes. This is performed with ArcGIS Pro, based on the three land cover classification images. Firstly, the images were converted from raster to polygon to be able to calculate the area of each of the classes. Subsequently, changes between the two years were calculated using the 'intersect' analysis tool from geoprocessing. Finally, in the attribute table of the resulting layer, two new fields were created: 'change' to identify the former and new cover types and 'area changes' to calculate the geometric difference between them.

4 Results

This section presents the outcomes of land cover analysis in Hanoi using the images from 2000, 2010 and 2022. The MLC method was employed to classify the images into four classes: water, built-up land, green areas and barren land. These resulting maps and their respective accuracy assessments will be presented. The study also illustrates the NDVI results, defining the threshold to differentiate three classes: water, non-vegetated, and vegetated areas for the images from 2010 and 2022. Furthermore, the study presents the land cover changes for each class and quantifies these changes.

4.1 Maximum Likelihood Classification and Accuracy Assessment

A land cover analysis was conducted for Hanoi using the spectral bands of the Landsat images of 2000, 2010 and 2022 and the MLC algorithm. The resulting land cover maps show four distinct classes: water, built-up land, green areas, and barren land (Figure 9). Through the visual examination and comparison of these maps, it becomes evident that changes in land cover can be observed from 2000 to 2022. The substantial transformation observed in the built-up cover class over this period is particularly noteworthy. Furthermore, visual analysis reveals that these expansions predominantly occur within pre-existing built-up areas.

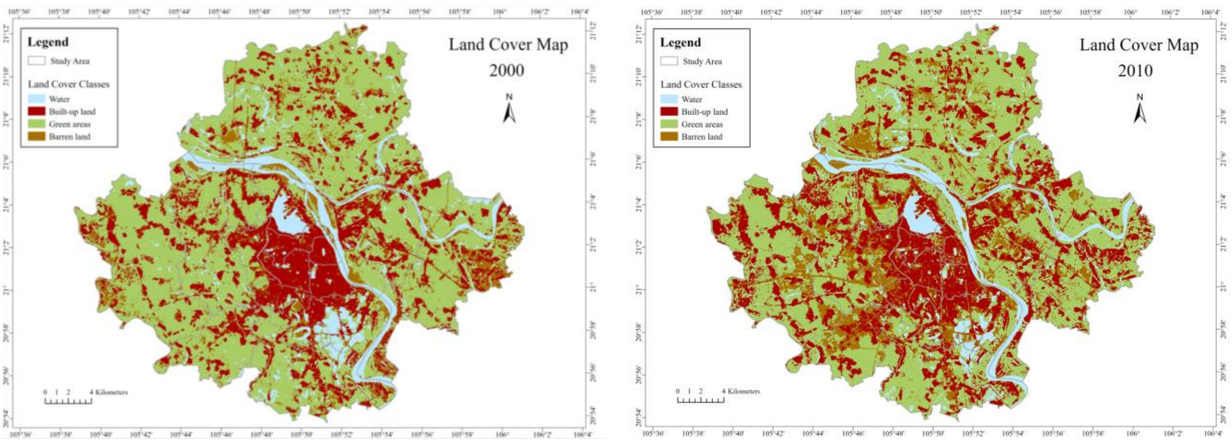

a) b)

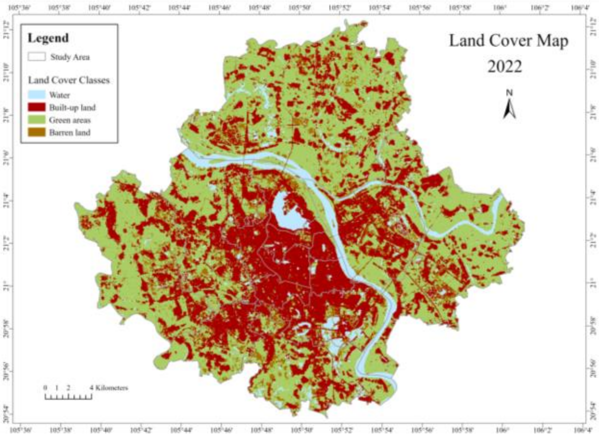

c)

Figure 9. Land cover maps of Hanoi using the MLC: a) 2000; b) 2010; c) 2022.

For the previous land cover maps, the area for every class was calculated (Table 10).

Table 9. Area coverage by square kilometres for the land cover classes in 2000, 2010 and 2022.

Land cover class	2000		2010		2022	
	(Km^2)	(%)	(Km^2)	(%)	(Km^2)	(%)
Water	74.32	9.94	64.94	8.68	59.16	7.91
Built-up land	178.11	23.82	201.74	26.99	255.01	34.10
Green areas	442.63	59.19	386.71	51.72	378.83	50.66
Barren land	52.79	7.05	94.46	12.63	54.85	7.33

An accuracy assessment was conducted for each of the land cover maps to examine how well the performance of the MLC algorithm was. The overall accuracy obtained using the MLC method was 79, 84, and 84 per cent for the years 2000, 2010 and 2022, respectively. However, chapter 3.5 explains that examining each class's user and producer accuracies is crucial. The MLC method showed strong performance in mapping green areas, indicated by higher user's accuracy percentages of 92, 96 and 90 for the three images. A high user's accuracy indicates a low commission error, meaning there is a high probability that pixels classified as green areas exist on the ground (Story and Congalton, 1986). However, the producer's accuracy in this class was slightly lower, at 73, 88 and 87 per cent, respectively. The producer's accuracy defines the possibility that this class's ground reference points were classified as correct (Story & Congalton, 1986). The performance of the MLC in mapping the water class showed more significant variability, as users' accuracies ranged from 61 to 82 per cent; however, the producer's accuracy for this class was 85 per or higher. The principal difficulty in accurately classifying this particular land cover category was the extensive presence of rice fields within the study area, which resemble water surfaces, producing errors between these two classes. The user's accuracy in mapping built-up land was 79, 81, and 88 per cent for the three images, and the producer's accuracy was 90, 76 and 86 per cent. The performance of MLC in classifying barren land exhibited significant limitations, as the user's accuracy did not surpass 42% across all the images analyzed. Moreover, this class had high omission errors, showed by a low producer's accuracy. For example, the producer's accuracy in the barren land class is 67, 79 and 36 per cent for the three images. These low figures compared to the other producer's accuracy may be attributed to the limited number of training samples available for the barren land class compared to other classes. Notably, the image from 2010, which had more training samples for the barren class, resulted in the highest user's accuracy compared to the images from 2000 and 2022. Likewise, a larger quantity of training samples was employed for the green areas class in all the images, leading to the highest user's accuracy for that specific land cover category. The complete confusion matrices for the accuracy assessment of the land cover maps from the Landsat images 2000, 2010 and 2022 are presented below (Tables 11-13).

Table 10. Accuracy assessment of land cover map 2000.

Classified	**Reference data**				**Total**	**User's accuracy**
	Water	Built-up land	Green areas	Barren land		
Water	17	0	11	0	28	61%
Built-up	1	52	11	2	66	79%
Green areas	1	5	85	1	89	92%
Barren land	1	1	9	6	17	35%
Total	20	58	113	9	200	
Producer's accuracy	85%	90%	73%	67%		
					Overall accuracy	**79%**
					Kappa	**0.66**

Table 11. Accuracy assessment of land cover map 2010.

Classified	**Reference data**				**Total**	**User's accuracy**
	Water	Built-up land	Green areas	Barren land		
Water	14	1	1	1	17	82%
Built-up	0	44	9	1	54	81%
Green areas	1	2	99	1	103	96%
Barren land	1	11	3	11	26	42%
Total	16	58	112	14	200	
Producer's accuracy	88%	76%	88%	79%		
					Overall accuracy	**84%**
					Kappa	**0.74**

Table 12. Accuracy assessment of land cover map 2022.

Classified	**Reference data**				**Total**	**User's accuracy**
	Water	Built-up land	Green areas	Barren land		
Water	12	0	4	0	16	75%
Built-up	2	60	2	4	68	88%
Green areas	0	7	91	3	101	90%
Barren land	0	3	8	4	15	27%
Total	14	70	105	11	200	
Producer's accuracy	86%	86%	87%	36%		
					Overall accuracy	**84%**
					Kappa	**0.73**

4.2 NDVI

According to Asrar et al. (1984), vegetation indices show better sensitivity than individual spectral bands for vegetation detection. This characteristic makes them highly valuable for enhancing classifications in thematic mapping (Asrar et al., 1984). Therefore, a map showing the NDVI values for each image was performed (Figure 10). The NDVI values range from - 0.125 to 0.487 for the 2000 image, from -0.109 to 0.430 for 2010 and from -0.173 to 0.485 for 2022. Negative values represent water, while positive values indicate a transition from non-vegetated to vegetated areas. When observing the maps, it can be seen that the 2000 image contained more values approaching the higher range, representing vegetated areas (shown in green) than the other two images, particularly in the northern and western regions of the study area. However, the 2022 image displayed higher values in the eastern part of the study area relative to the other two images. Furthermore, the area representing medium values (indicated by orange) representing non-vegetated areas was found to have increased from 2000 to 2022.

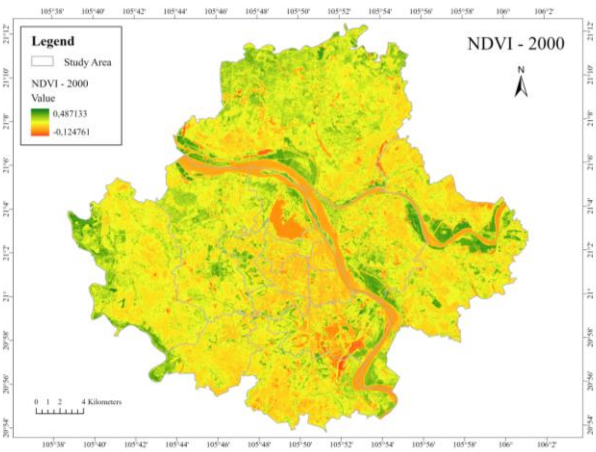

a)

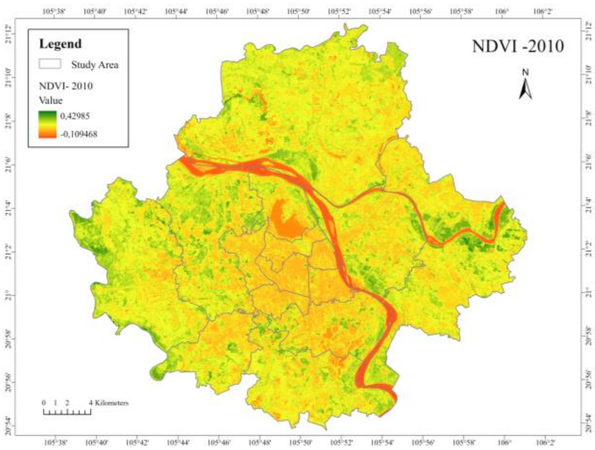

b)

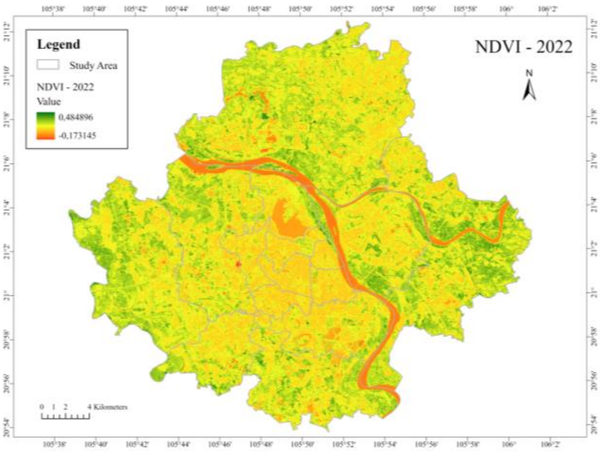

c)

Figure 10. NDVI values from the Landsat images: a) 2000; b) 2010; c) 2022.

The following land cover maps for 2010 and 2022 were created based on the NDVI values (Figure 11). These maps were classified into three categories: water, non-vegetated, and vegetated areas, which were established after manually inspecting the pixel values of the images and defining the thresholds for each land cover class. The research within this study showed that the NDVI values for water were from negative values up to 0.031, the non-vegetated areas were within the range between 0.032 and 0.141, and the vegetated areas were above 0.142 up to the higher value of 0.43 in the case of the 2010 image. For the image 2022, the NDVI values for water ranged from negative values up to 0.029, the non-vegetated areas were within the range between 0.03 and 0.153, and the vegetated areas were above 0.154 up to the higher value of 0.485.

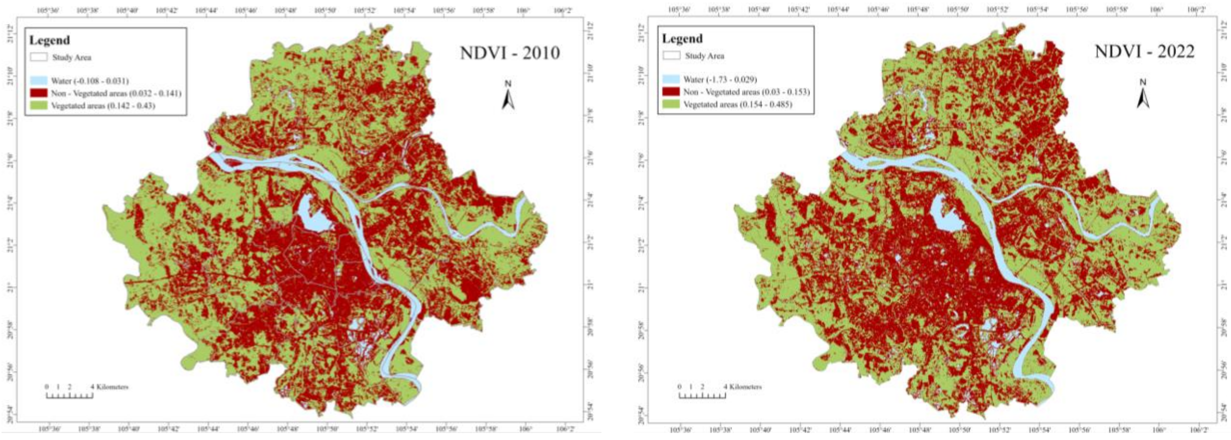

a) b)

Figure 11. NDVI-2022 with the thresholds for each class.

The accuracy assessment for the classification maps from 2010 and 2022 obtained from the NDVI values was performed. The overall accuracies obtained for the maps were 74 and 82 per cent for the 2010 and 2022 images. The user's accuracy for the water class was 100 per cent for both images; however, the producer's accuracy for this class did not exceed 70 per cent. The classification of vegetated areas demonstrated higher accuracy than non-vegetated areas, which exhibited significant commission errors, indicated by a user's accuracy of 59 per cent for the 2010 image and 74 per cent for the 2022 image. The results for the vegetated areas accuracies were higher than 80 per cent, except for the producer's accuracy for the image 2010, which was 73 per cent. The complete confusion matrices are shown below (Tables 14 - 4.6).

Table 13. Accuracy assessment of NDVI classification from Landsat 2010.

Land cover class	**Reference data**			**Total**	**User's accuracy**
	Water	Non-vegetated areas	Vegetated areas		
Water	13	0	0	13	100%
Non-vegetated areas	5	52	31	88	59%
Vegetated areas	3	13	83	99	84%
Total	17	73	13	200	
Producer's accuracy	62%	80%	73%		
				Overall accuracy	**74%**
				Kappa	**0.54**

Table 14. Accuracy assessment of NDVI classification from Landsat 2022.

Land cover class	**Reference data**			**Total**	**User's accuracy**
	Water	Non-vegetated areas	Vegetated areas		
Water	15	0	0	15	100%
Non-vegetated areas	5	67	18	90	74%
Vegetated areas	2	12	82	96	85%
Total	17	73	13	200	
Producer's accuracy	68%	85%	82%		
				Overall accuracy	**82%**
				Kappa	**0.68**

The land cover classification maps derived from NDVI values and the MLC method were utilized to calculate the areas of the three classes, facilitating a comparison between the results obtained from both classifications (Table 16). The total area of the study region has an extension of 747.9 square kilometres. In the MLC classification, the non-vegetated areas are equivalent to the combined sum of built-up and barren land classes. Comparisons reveal variations in the area estimates obtained through the two classifications. With the NDVI classification, the non-vegetated class obtained a larger extension of 32.8 and 26.74 square kilometres in 2010 and 2022, respectively, compared to the areas obtained from the MLC classification. Moreover, the vegetated areas obtained through the NDVI classification were 16.26 and 21.43 square kilometres less in 2010 and 2022, respectively, compared to the results obtained through MLC. In the water class, the area obtained from the NDVI classification was 16.48 square kilometres lower in 2010 and 5.27 larger in 2022 compared to the figures obtained from the MLC classification.

Table 15. Area results for 2010 and 2022 images were obtained from two NDVI and MLC classifications.

Land cover classes	**2010**				**2022**			
	NDVI		MLC		NDVI		MLC	
	Km^2	%	Km^2	%	Km^2	%	Km^2	%
Water	48.52	6.49	64.94	8.68	53.67	7.18	59.16	7.91
Non-vegetated areas	328.91	43.98	296.20*	39.61	336.68	45.02	309.86**	41.43
Vegetated areas	370.42	49.53	386.71	51.71	357.50	47.80	378.83	50.66

*296.20 = 201.74 (Built-up land) + 94.46 (Barren land)

**309.86 = 255.01 (Built-up land) + 54.85 (Barren land)

4.3 Post-processing

The images obtained from the classification show some salt-and-pepper noise, which was reduced by performing the majority filter. An example of how it is seen in an image before and after performing the majority filter is shown below (Figure 12).

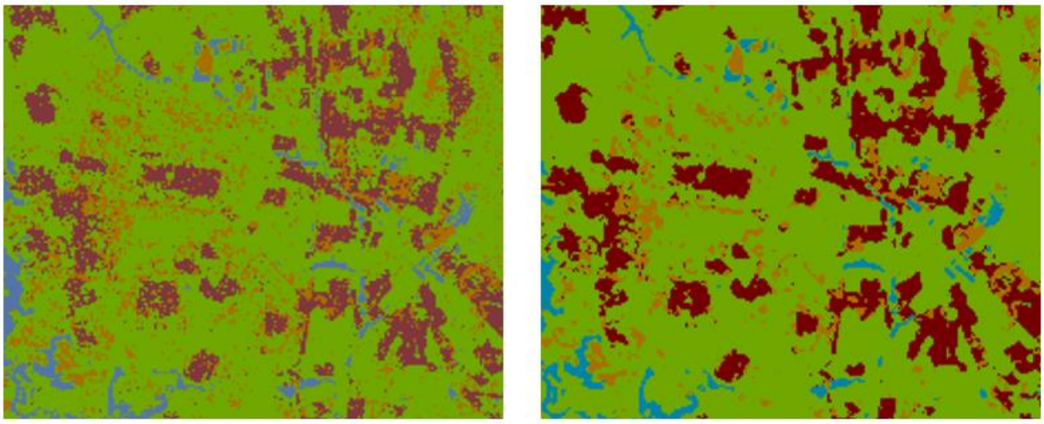

a) b)

Figure 12. Post-classification smoothing: a) original classification; b) smoothed using majority filter.

4.3 Land Cover Change Detection

This section presents the outcomes derived from the analysis of land cover change. The classified land cover maps generated through the MLC method for Hanoi were employed to identify and extract the dynamic changes occurring in Hanoi between two time periods: 2000 and 2010 (Figure 4.5) and from 2010 to 2022 (Figure 13).

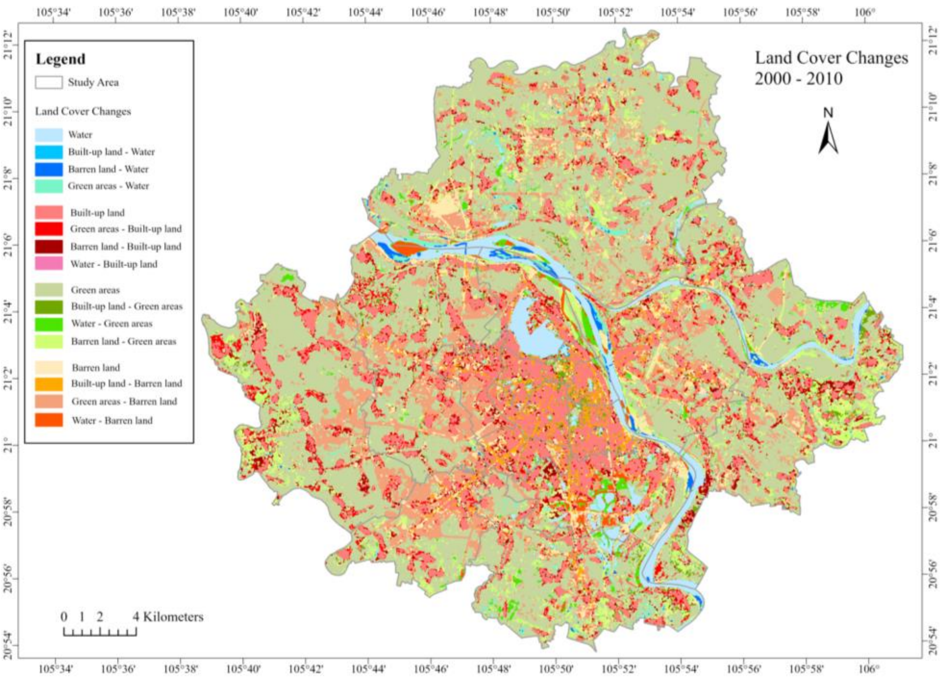

Figure 13. Land cover changes map from 2000 - 2010.

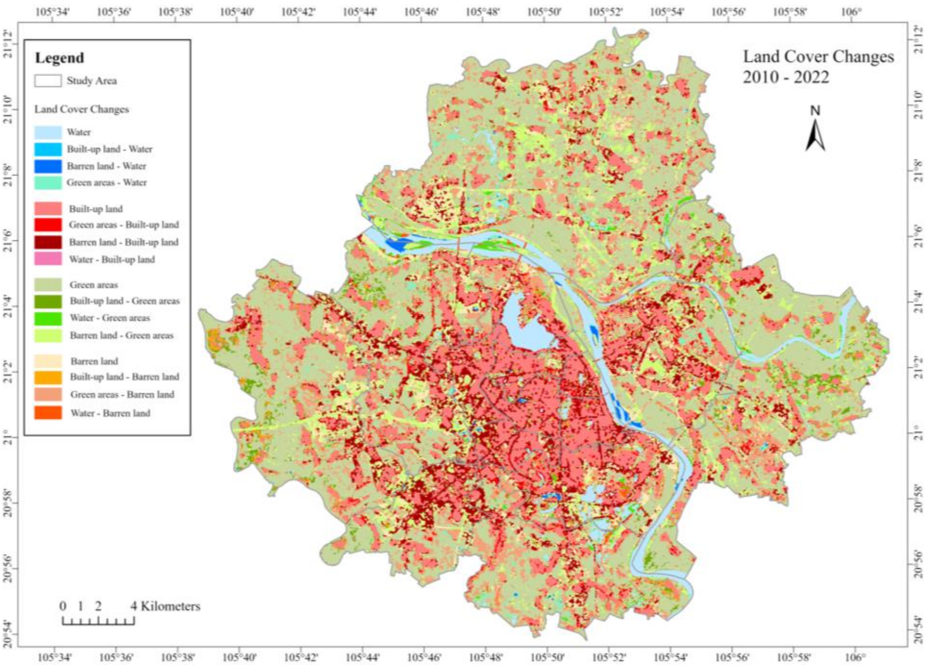

Figure 14. Land cover changes map from 2010 - 2022.

From 2000 to 2010, significant transformations in land cover were observed within the green areas. Approximately 13 per cent was converted into barren land, covering an extension of around 58 square kilometres. Moreover, 10 per cent of the total extension of the green areas was transformed into built-up areas, covering an extension of around 44 square kilometres, which resulted in an increase of 22 per cent in the built-up land. From 2010 to 2022, there was a decline in green area extension, resulting in the transformation into different land cover classes. Approximately 9 per cent was converted into barren land, covering an extension of around 34 square kilometres. Additionally, 10 per cent changed into built-up areas, covering an extension of 38 square kilometres, which resulted in an increase of around 15 per cent in the built-up land. It can also be seen that there was barren land converted into built-up areas, around 50 square kilometres, representing almost 20 per cent of the built-up extension (Figure 15).

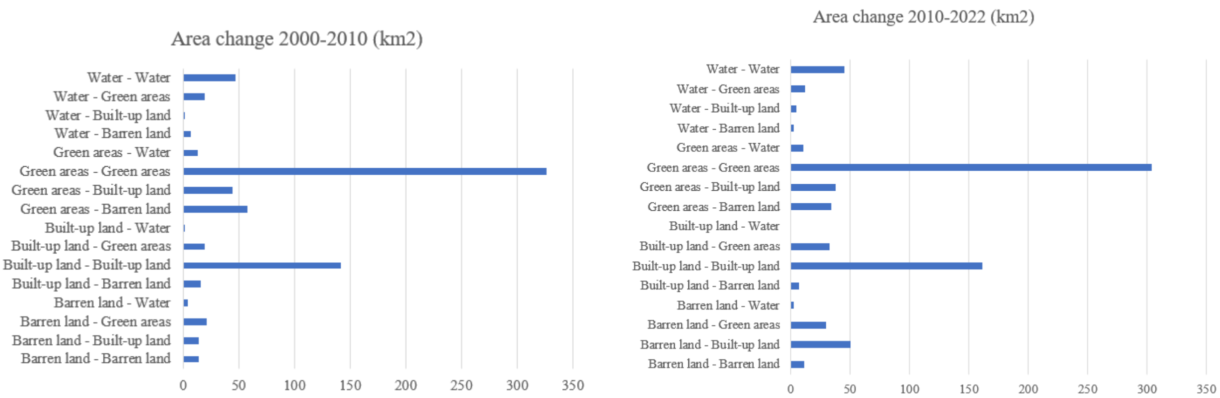

a) b)

Figure 15. Area chage a) 2000-2010; b) 2010-2022.

The table below expresses all the changes in the different land cover classes (Table 17).

Table 16. Land cover change areas from 2000 to 2010 and 2010 to 2022.

Land Cover Change	Area change 2000-2010 (km2)	Area change 2010-2022 (km2)
Water - Water	46,77	45,11
Water - Built-up land	1,71	5,01
Water - Green areas	18,92	12,01
Water - Barren land	6,87	2,77
Built-up land - Water	1,14	0,41
Built-up land - Built-up land	141,57	161,57
Built-up land - Green areas	19,70	32,88
Built-up land - Barren land	15,63	6,80
Green areas - Water	13,20	10,76
Green areas - Built-up land	44,26	38,07
Green areas - Green areas	326,82	303,68
Green areas - Barren land	58,055	33,88
Barren land - Water	3,78	2,83
Barren land - Built-up land	14,12	50,28
Barren land - Green areas	20,97	29,96
Barren land - Barren land	13,86	11,35

To better visualize the expansion of built-up areas, two maps were generated. The light red symbolizes the built-up land extension with no changes during the period frame, and the red symbolizes the increased built-up areas (Figures 16 - 17). It can be seen that the expansion of built-up land was more significant during the period between 2010 and 2022 than in the one between 2000 and 2010. Furthermore, most modified areas were located close to the existing built-up areas.

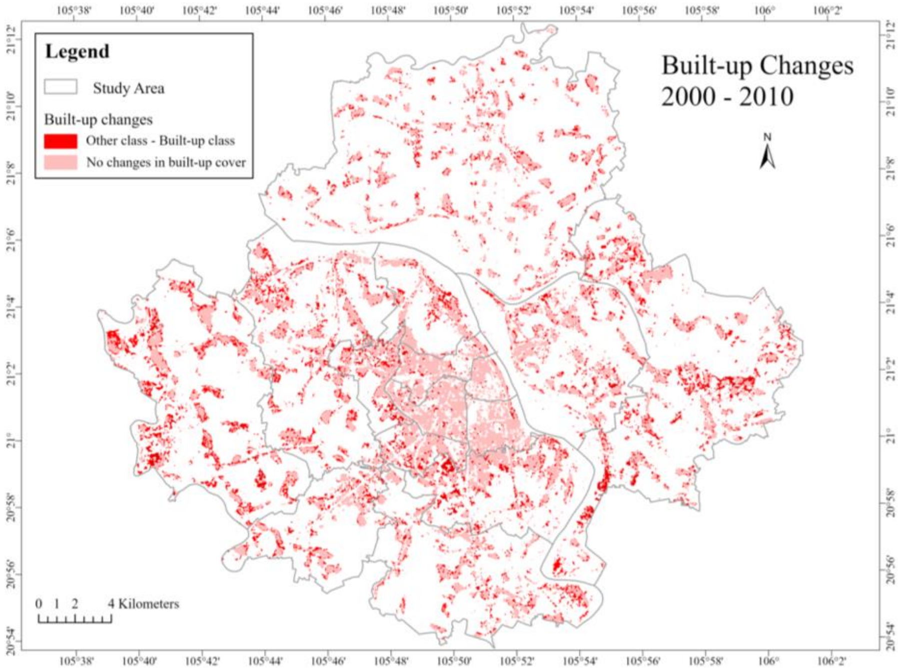

Figure 16. Built-up changes from 2000 to 2010.

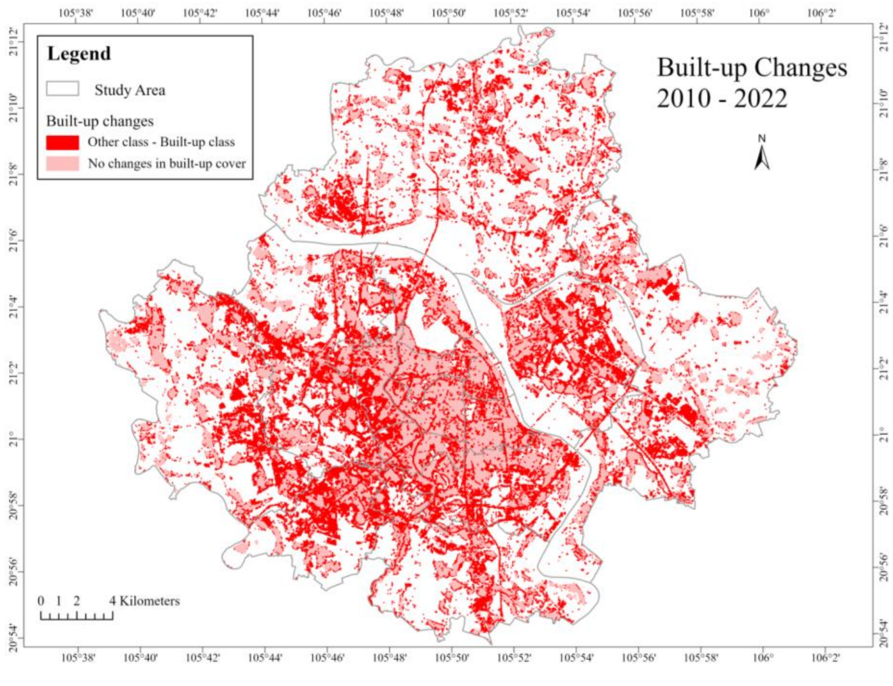

Figure 17. Built-up changes from 2010 to 2022.

The areas of built-up and green cover classes were quantified for three years, enabling an evaluation of the magnitude of changes within these classes (Table 18).

Table 17. Built-up and green areas. Built-up expansion and greenery reduction expressed in km^2.

Cover land	2000	2010	2022	2000-2010	2010-2022
Built-up land	178.11	201.74	255.04	+ 23.63	+ 53,30
Green areas	442.63	386.71	378.83	- 55.92	- 7.88

5. Discussion

5.1 Alternative Data for the Study

For this study, the use of Sentinel-2 data was considered a possibility at first because of the higher spatial resolution compared to Landsat data, 10 and 30 meters, respectively, being possible to obtain higher accurate results according to some studies such as the one from Phiri et al. (2020). Since the Sentinel-2 mission was launched in 2015, the first image considered to use in the study was from this year, together with an image from 2017, 2019 and 2022 with a cloud cover of less than 5%, acquired freely from Copernicus Open Access Hub (https://scihub.copernicus.eu/dhus/). Unfortunately, the images from 2015 and 2017 were only available from level 1C, which means that the images are from Top-Of-Atmosphere (TOA) and are not atmospheric corrected yet. However, the software Sentinel Application Platform (SNAP) with the Sen2Cor plugin can be used for performing atmospheric correction (Rumora et al., 2020). SNAP software provided by the European Space Agency (ESA) can be freely downloaded from SNAP Download – STEP (esa. int) and is a tool for processing data products from several remote-sensing missions, including Sentinel-1, Sentinel-2 and Sentinel-3 (ESA, n.d.). On the contrary, the images from 2019 and 2022 were available from level 2A, meaning that these images are from Bottom-Of-Atmosphere (BOA), being corrected reflectance products and ready to work with. Unfortunately, the use of SNAP software is beyond the capacity of this study. Attempts to convert the images from 2015 and 2017 from TOA to BOA were unsuccessful. As a result, only images from 2019 and 2022 could be used, assuming the hypothesis that no noteworthy changes could be detected over the limited time frame. That is why the selection of images from Landsat imagery was chosen, being more flexible with the range of years for the study.

5.2 Ancillary Data

Examining the accuracy assessment of the land cover classification maps obtained from using the spectral bands of Landsat images reveals the potential for improved accuracy. As highlighted by Janssen et al. (1990), image classification based only on spectral observations is often not enough to obtain sufficiently accurate results, being helpful with the incorporation of additional geospatial data, such as the digital elevation model (DEM). This attempt was tried to enhance the accuracy of the classification. For that, DEM data was freely downloaded from EarthExplorer (usgs.gov). Three rasters were downloaded to cover the entire study area and mosaicked into a single image, followed by clipping to the study area extent. The DEM raster had an original cell size of 27.7 meters, which required resampling to match the 30-meter cell size of the Landsat images. Unfortunately, due to pixel mismatch between the digital elevation model (DEM) and Landsat raster data when they overlapped, it was not feasible to create a single raster dataset. Despite attempts to address this issue, a solution could not be found, resulting in excluding the DEM data from this study.

5.3 NDVI

This study generated land cover maps based on NDVI values by manually examining pixel values and determining corresponding thresholds for each land cover class. The aim was to evaluate the accuracy of this approach to see how well it could classify land cover. However, the results obtained were inferior to those achieved through a supervised classification method except for the class water, which obtained a user's accuracy of 100 per cent; however, the producer's accuracy for this class was also inferior. For example, in vegetated areas for the 2010 image, the user's accuracy obtained from the supervised method was 96 per cent compared to 84 per cent obtained from the NDVI classification. In addition, in numerous instances, pixels representing vegetated areas had values close to zero, making it challenging to establish a suitable threshold. It was impossible to establish such a low threshold for the vegetated areas because, in this way, many non-vegetated areas would be defined erroneously as vegetated. Consequently, this fact led to reduced accuracy.

The NDVI was utilized to assess the accuracy of generating classification maps by establishing thresholds for the different classes. However, since the results obtained from the 2010 and 2022 images did not reach the desired accuracies, confirming that the classification was not significantly better than the one obtained by the supervised method, the classification with NDVI values for the 2000 image was not performed.

Many land cover classification studies include one or more vegetation index measures in their data to improve the identification of vegetation cover. For example, Manandhar et al. (2009) demonstrated that incorporating the NDVI value of the Landsat imagery into the post-classification correction made it possible to improve MLC maps significantly, and Akar and Gungor (2015) also used NDVI in the classification process to enhance classification accuracy. However, further research is required to comprehend how NDVI can improve the accuracy of MLC maps since this particular approach was not undertaken in the current study.

5.4 Accuracy Assessment

The accuracy assessment can be conducted using different sampling strategies (Esri, n.d.-a). The stratified random strategy is the one that was chosen for this study. However, the equalized stratified random was also attempted for the 2022 image to compare the results (Table 19) based on the recommendation of Congalton (1988), who suggested a minimum of 50 samples per class for assessing the accuracy of classification maps. As the chosen number of points for the assessment was 200 and there were four classes, there was a guarantee of obtaining 50 samples per class. With this sampling strategy, the overall accuracy was lower (73 per cent) than the stratified random strategy (84 per cent). However, the user's accuracies were higher than in the stratified random strategy except for the user's accuracy for water, which was the same in both cases. The user's accuracy obtained from stratified random strategy was: water 75 per cent, built-up 88 per cent, green areas 90 per cent, and barren 27 per cent. Comparing the producer's accuracy, the values obtained with the stratified random strategy were 86 per cent for water, 86 per cent for built-up land, 87 per cent for green areas and 36 per cent for barren land.

Table 18. Accuracy assessment of land cover classification 2022, performing an equalized stratified random strategy.

Classified	**Reference data**				**Total**	**User's accuracy**
	Water	Built-up land	Green areas	Barren land		
Water	41	2	6	1	50	82%
Built-up	1	45	3	1	50	90%
Green areas	2	1	45	2	50	90%
Barren land	2	13	21	14	50	28%
Total	46	61	75	18	200	
Producer's accuracy	89%	74%	60%	78%		
					Overall accuracy	**73%**
					Kappa	**0.63**

Therefore, it can be seen that in these accuracies, there are significant differences, especially in the green areas and in the barren land. However, considering the statement by Congalton and Green (2019), who say that the number of samples per class should be adjusted based on the importance of the specific class for the project, there was considered more appropriate to employ the stratified random strategy. Nonetheless, it should be acknowledged that the results of the different accuracies can vary significantly depending on the selected strategy.

Another noteworthy observation regarding the accuracy assessment is that the classes demonstrating higher accuracy are those that have been assigned a greater number of training samples. Therefore, to potentially improve these results, incorporating supplementary samples could be considered to enhance the classification accuracy outcomes.

5.5 Land Cover Changes

Examining the outcomes derived from the analysis of land cover changes during the two periods, it was not possible to determine the level of accuracy of these changes. These results were derived from the MLC maps, which showed low user's accuracies in the barren land class and user's accuracies inferior to 80 per cent in the water class in 2000 and 2022. Consequently, the reliability of changes involving these two classes was diminished. Furthermore, the land cover change from built-up land to green areas, comprising almost 20 square kilometres in 2000-2010 and around 33 square kilometres in 2010-2022, appears to be questionable.

5.6 Supervised Classification Methods

The study also considered the possibility of employing alternative classification methods to evaluate their potential for achieving improved land cover classification results. The original intention was to compare the performance of various supervised classification methods, including Random Forest and

Support Vector Machine (SVM), in addition to MLC. However, conducting these intended comparisons was not feasible due to time limitations.

6. Conclusion and Future Outlook

The use of GIS and remote sensing techniques for land cover monitoring has been extensively demonstrated in many scholarly works, including Mauro, 2020, Shandas et al. (2017), Kumar et al. (2020), Nong et al. (2015) and Duan and Shibayama (2009), among numerous others. This approach has been established as a viable method. However, the exclusive reliance on spectral bands for mapping different land cover classes can be challenging, particularly in the case of certain classes, as could be seen in this case study, where the overall accuracy is around 80 per cent for the three images in the study and user and producer accuracies ranging from 73 to 90 per cent for most classes, Notably, the accuracy of the barren class produces unsatisfactory results. Based on these findings, it is deduced that incorporating additional data to the spectral bands could potentially enhance these outcomes.

The application of NDVI classification as an approach for land cover classification, specifically in detecting class-specific thresholds, did not produce significant results, as observed from the accuracy assessment. Therefore, it is concluded that NDVI should be utilized as ancillary data for post-classification enhancement rather than relying solely on it for classifying land cover classes.

This study examined the land cover changes in Hanoi, using satellite data from 2000 to 2022. The results suggest that the urban areas in Hanoi have increased 24 square kilometres over the first ten years of study and 54 square kilometres in the next 12 years of study. The physical growth of Hanoi can be appreciated by analysing satellite images. Therefore the chosen method for detecting land cover changes proved to be suitable, as it enabled comprehensive visualization of changes across each land cover class and quantification of the spatial extent in square kilometres of transformations from one land cover category to another.

For future outlook, it would be interesting to incorporate population census data as ancillary information to detect density growth and examine the expansion of built-up areas concerning population dynamics. Understanding the extent and density of population changes is crucial for effective urban planning. Integrating population census data would provide valuable insights into the spatial distribution of population growth, enabling a more comprehensive analysis of urban development patterns.

References

ADB and IDB. (2014). *SuStainable urbanization in aSia and latin america*. www.iadb.org

Akar, & Güngör, O. (2015). Integrating multiple texture methods and NDVI to the Random Forest classification algorithm to detect tea and hazelnut plantation areas in northeast Turkey. *International Journal of Remote Sensing*, *36*(2), 442–464. https://doi.org/10.1080/01431161.2014.995276

Anderson, J. R., Hardy, E. E., Roach, J. T., & Witmer, R. E. (1983). *A Land Use and Land Cover Classification System for Use with Remote Sensor Data*. 8.

Asrar, G., Fuchs, M., Kanemasu, E. T., & Hatfield, J. L. (1984). Estimating Absorbed Photosynthetic Radiation and Leaf Area Index from Spectral Reflectance in Wheat 1 . *Agronomy Journal*, *76*(2), 300–306. https://doi.org/10.2134/AGRONJ1984.00021962007600020029X

Bhandari, A. K., Kumar, A., & Singh, G. K. (2012). Feature Extraction using Normalized Difference Vegetation Index (NDVI): a Case Study of Jabalpur City. *Procedia Technology*, *6*, 612–621. https://doi.org/10.1016/j.protcy.2012.10.074

Boudreau, J.-A., & Geertman, S. (2015). *Youth-friendly public spaces in Hanoi*. https://www.academia.edu/88528123/Youth_friendly_public_spaces_in_Hanoi

Congalton, R. G. (2001). Accuracy assessment and validation of remotely sensed and other spatial information. *International Journal of Wildland Fire*, *10*(3–4), 321–328. https://doi.org/10.1071/WF01031

Congalton, R. G., & Green, K. (2019). *Assessing the accuracy of remotely sensed data: principles and practices* (Third Edition). https://dokumen.pub/qdownload/assessing-the-accuracy-of-remotely-sensed-data-principles-and-practices-thirdnbsped-9781498776660-1498776663.html

Congalton. Russell.G. (1988). A Comparison of Sampling Schemes Used in Generating Error Matrices for Assessing the Accuracy of Maps Generated from Remotely Sensed Data. *Photogrammetric Engineering and Remote Sensing*, *54*(5), 593–600.

Dean, A. M., & Smith, G. M. (2003). An evaluation of per-parcel land cover mapping using maximum likelihood class probabilities. *International Journal of Remote Sensing*, *24*(14), 2905–2920. https://doi.org/10.1080/01431160210155910

Duan, D. H., & Shibayama, M. (2009). *Studies on Hanoi Urban Transition in the Late 20th Century Based on GIS/RS*. https://www.researchgate.net/publication/40269917_Studies_on_Hanoi_Urban_Transition_in_the_Late_20th_Century_Based_on_GISRS

Dunlap, R. E., & Jorgenson, A. K. (2012). Environmental Problems. *The Wiley-Blackwell Encyclopedia of Globalization*. https://doi.org/10.1002/9780470670590.WBEOG174

Economist Intelligence Unit (EIU). (2011). *Asian Green City Index*. Siemens AG.

Enderle, D. I., Weih Jr, R. C., Jr, R. C., IMEnderle, D., & WeihJr, R. C. (2005). Integrating Supervised and Unsupervised Classification Methods to Develop a More Accurate Land Cover Classification. *Journal of the Arkansas Academy of Science*, *59*, 10. http://scholarworks.uark.edu/jaashttp://scholarworks.uark.edu/jaas/vol59/iss1/10

ESA. (n.d.). *SNAP spurs Earth observation innovation with one million downloads*. Retrieved May 9, 2023, from https://www.esa.int/Applications/Observing_the_Earth/FutureEO/SNAP_spurs_Earth_observation_innovation_with_one_million_downloads

Esri. (n.d.-a). *Accuracy Assessment*. Retrieved May 21, 2023, from https://pro.arcgis.com/en/pro-app/latest/help/analysis/image-analyst/accuracy-assessment.htm

Esri. (n.d.-b). *Majority Filter (Spatial Analyst)*. Retrieved April 18, 2023, from https://pro.arcgis.com/en/pro-app/latest/tool-reference/spatial-analyst/majority-filter.htm

Foody, G. M. (2020). *Explaining the unsuitability of the kappa coefficient in the assessment and comparison of the accuracy of thematic maps obtained by image classification*. https://doi.org/10.1016/j.rse.2019.111630

Gao, Y., & Mas, F. J. (2008). A comparison of the performance of pixel based and object based classifications over images with various spatial resolutions. *OnLine Journal of Earth Sciences*, *2*(1), 27–35. https://www.researchgate.net/publication/261286350_A_comparison_of_the_performance_of_pixel_based_and_object_based_classifications_over_images_with_various_spatial_resolutions

General Statistics Office (GSO). (n.d.). *General Statistics Office of Vietnam*. Retrieved April 27, 2023, from https://www.gso.gov.vn/en/about-gso/

Gong, F., & Liu, Q. (2023). *Monitoring land use and land cover change: a combining approach of change detection to analyze urbanization in Shijiazhuang, China*.

Janssen, L. L. F., Jaarsma, M. N., & Van Der Linden, E. T. M. (1990). *Integrating Topographic Data with Remote 1 Sensing for and-Cover Classification*.

Japan International Cooperation Agency (JICA). (2007). *The Comprehensive Urban Development Programme in Hanoi Capital City of the Socialist Republic of Vietnam*.

Kien, T. N., & Heo, Y. (2008). Doi Moi Policy and Socio-Economic Development in Vietnam, 1986–2005. *International Area Studies Review*, *11*(1), 205–232. https://doi.org/10.1177/223386590801100112

Kshetri, T. B. (2018). NDVI, NDBI & NDWI Calculation Using Landsat 7, 8. *Geomatics for Sustainable Development*, *II*, 32–34.

https://www.researchgate.net/publication/327971920_NDVI_NDBI_NDWI_Calculation_Using_Landsat_7_8

Kumar, S., Shwetank, & Jain, K. (2020). A Multi-Temporal Landsat Data Analysis for Land-use/Land-cover Change in Haridwar Region using Remote Sensing Techniques. *Procedia Computer Science*, *171*, 1184–1193. https://doi.org/10.1016/J.PROCS.2020.04.127

Labbé, D. (2010). *Facing the urban transition in Hanoi: recent urban planning issues and initiatives*.

Labbé, D. (2021). Urban transition in Hanoi : huge challenges ahead. In *Trends in Southeast Asia* (Issue 2).

Lillesand, T. M., Kiefer, R. W., & Chipman, J. W. (2015). *REMOTE SENSING AND IMAGE INTERPRETATION* (Seventh edition).

Liou, Y. A., Nguyen, K. A., & Ho, L. T. (2021). Altering urban greenspace patterns and heat stress risk in Hanoi city during Master Plan 2030 implementation. *Land Use Policy*, *105*. https://doi.org/10.1016/J.LANDUSEPOL.2021.105405

Luan, T. D. (2014). Living in “New Urban Areas”: towards sustainable urban communities in Hanoi, Vietnam. *Transactions on Ecology and The Environment*, *181*, 1743–3541. https://doi.org/10.2495/EID140291

Luan, T. D., Vinh, N. Q., Wiesman, B., & Leaf, M. (2000). *Socioeconomic Renovation in Viet Nam: The Origin, Evolution, and Impact of Doi Moi | IDRC - International Development Research Centre: Vol. Part II* (P. Boothroyd & P. X. Nam, Eds.). https://www.idrc.ca/en/book/socioeconomic-renovation-viet-nam-origin-evolution-and-impact-doi-moi

Maclean, M. G., Campbell, M. J., Maynard, D. S., Ducey, M. J., & Congalton, R. G. (2013). Requirements for labelling forest polygons in an object-based image analysis classification. *International Journal of Remote Sensing*, *34*(7), 2531–2547. https://doi.org/10.1080/01431161.2012.747017

Manandhar, R., Odehi, I. O. A., & Ancevt, T. (2009). Improving the accuracy of land use and land cover classification of landsat data using post-classification enhancement. *Remote Sensing*, *1*(3), 330–344. https://doi.org/10.3390/RS1030330

Mauro, G. (2020). Rural–urban transition of hanoi (Vietnam): Using landsat imagery to map its recent peri-urbanization. *ISPRS International Journal of Geo-Information*, *9*(11). https://doi.org/10.3390/IJGI9110669

Nong, D. H., Fox, J., Miura, T., & Saksena, S. (2015). Built-up Area Change Analysis in Hanoi Using Support Vector Machine Classification of Landsat Multi-Temporal Image Stacks and Population Data. *Land*, *4*(4), 1213–1231. https://doi.org/10.3390/land4041213

Olofsson, P., Foody, G. M., Herold, M., Stehman, S. V., Woodcock, C. E., & Wulder, M. A. (2014). Good practices for estimating area and assessing accuracy of land change. *Remote Sensing of Environment*, *148*, 42–57. https://doi.org/10.1016/J.RSE.2014.02.015

Paul, S. S. (2008). *ANALYSIS OF LAND USE AND LAND COVER CHANGE IN KISKATINAW RIVER WATERSHED: A REMOTE SENSING, GIS & MODELING APPROACH*.

Pham, V. C., Pham, T. T. H., Tong, T. H. A., Nguyen, T. T. H., & Pham, N. H. (2015). The conversion of agricultural land in the peri-urban areas of Hanoi (Vietnam): patterns in space and time. *Journal of Land Use Science*, *10*(2), 224–242. https://doi.org/10.1080/1747423X.2014.884643

Phiri, D., Simwanda, M., Salekin, S., Nyirenda, V. R., Murayama, Y., & Ranagalage, M. (2020). Sentinel-2 Data for Land Cover/Use Mapping: A Review. *Remote Sensing 2020, Vol. 12, Page 2291*, *12*(14), 2291. https://doi.org/10.3390/RS12142291

Phuc, Q. N. (2013). AGRICULTURAL LAND CONVERSION FOR URBAN DEVELOPMENT: A CRITICAL ANALYSIS OF CONTEXT, DRIVERS, AND CONSEQUENCES IN VIETNAM. *Journal of Science, Hue University*, *80*(2), 147–159. https://www.researchgate.net/publication/318671652_AGRICULTURAL_LAND_CONVERSION_FOR_URBAN_DEVELOPMENT_A_CRITICAL_ANALYSIS_OF_CONTEXT_DRIVERS_AND_CONSEQUENCES_IN_VIETNAM

Phuong, L. T. M., Anh, V. Le, & Quang, N. H. (2021). Research on Urban Land Use Change in Ha Noi, Viet Nam Using Remote Sensing and GIS for Planning Oriented Work. *International Journal of Sustainable Construction Engineering and Technology*, *12*(3 Special issue), 24–34. https://doi.org/10.30880/IJSCET.2021.12.03.003

Rumora, L., Miler, M., & Medak, D. (2020). Impact of Various Atmospheric Corrections on Sentinel-2 Land Cover Classification Accuracy Using Machine Learning Classifiers. *Geo-Information*. https://doi.org/10.3390/ijgi9040277

Satellite Imaging Corporation. (2022). *Satellite Images*. https://www.satimagingcorp.com/gallery/high-resolution/

Shandas, V., Makido, Y., & Ferwati, S. (2017a). Rapid Urban Growth and Land Use Patterns in Doha, Qatar: Opportunities for Sustainability. *European Journal of Sustainable Development Research*, *1*(2), 11. https://doi.org/10.20897/ejosdr.201711

Shandas, V., Makido, Y., & Ferwati, S. (2017b). Rapid Urban Growth and Land Use Patterns in Doha, Qatar: Opportunities for Sustainability. *European Journal of Sustainable Development Research*, *1*(2), 11. https://doi.org/10.20897/ejosdr.201711

Storey, J., & Barsi, J. (2005). *LANDSAT 7 SCAN LINE CORRECTOR-OFF GAP-FILLED PRODUCT DEVELOPMENT*.

Story, M., & Congalton, R. G. (1986). Accuracy Assessment: A User's Perspective. *Photogrammetric Engineering and Remote Sensing*, *52*(3), 397–399.

Strahler, A. H., Boschetti, L., foody, giles M., Friedl, M. A., & Hansen Matthew C. (2006). *Global Land Cover Validation: Recommendations for Evaluation and Accuracy Assessment of Global Land Cover Maps*.

https://www.researchgate.net/publication/238580124_Global_Land_Cover_Validation_Recommendations_for_Evaluation_and_Accuracy_Assessment_of_Global_Land_Cover_Maps

Subha. (2020). *GIS and De-stripping (Gap Filling) - Split Tools In ArcGIS | GIS*. Agira- Innovation Engineered. https://www.agiratech.com/gis-and-de-stripping-gap-filling-split-tools-in-arcgis

The Central Census Steering Committee. (2010). *The 2009 Vietnam Population and Housing Census: Major Findings*.

The World Bank. (2023). *The World Bank in Vietnam*. https://www.worldbank.org/en/country/vietnam/overview

UN-Habitat. (2012). *SuStainable urbanization in aSia A Sourcebook for LocAL GovernmentS*.

United Nations. (2018a). *World Urbanization Prospects The 2018 Revision*.

United Nations. (2018b). *68% of the world population projected to live in urban areas by 2050, says UN | UN DESA | United Nations Department of Economic and Social Affairs*. https://www.un.org/development/desa/en/news/population/2018-revision-of-world-urbanization-prospects.html

USGS. (n.d.-a). *Landsat 5*. Retrieved April 8, 2023, from https://www.usgs.gov/landsat-missions/landsat-5

USGS. (n.d.-b). *Landsat 9*. Retrieved April 7, 2023, from https://www.usgs.gov/landsat-missions/landsat-9

USGS. (n.d.-c). *What are the band designations for the Landsat satellites?* Retrieved April 7, 2023, from https://www.usgs.gov/faqs/what-are-band-designations-landsat-satellites

USGS. (2020). *USGS EROS Archive - Landsat Archives - Landsat 7 ETM Plus Collection 2 Level-2 Science Products | U.S. Geological Survey*. https://www.usgs.gov/centers/eros/science/usgs-eros-archive-landsat-archives-landsat-7-etm-plus-collection-2-level-2

Weber, C., & Puissant, A. (2003). Urbanization pressure and modeling of urban growth: Example of the Tunis Metropolitan Area. *Remote Sensing of Environment*, *86*(3), 341–352. https://doi.org/10.1016/S0034-4257(03)00077-4

Word Population Review. (2023). *Hanoi Population 2023*. https://worldpopulationreview.com/world-cities/hanoi-population

Zanter, K. (2021). *LSDS-1618 Landsat 4-7 Collection 2 (C2) Level 2 Science Product (L2SP) Guide*.

Zhu, Z., Wulder, M. A., Roy, D. P., Woodcock, C. E., Hansen, M. C., Radeloff, V. C., Healey, S. P., Schaaf, C., Hostert, P., Strobl, P., Pekel, J. F., Lymburner, L., Pahlevan, N., & Scambos, T. A. (2019). Benefits of the free and open Landsat data policy. *Remote Sensing of Environment*, *224*, 382–385. https://doi.org/10.1016/J.RSE.2019.02.016